

Targeting the cytoplasmic polyadenylation element-binding protein CPEB4 protects against diet-induced obesity and microbiome dysbiosis



Nuria Pell¹, Ester Garcia-Pras¹, Javier Gallego¹, Salvador Naranjo-Suarez¹, Alexandra Balvey¹, Clara Suñer², Marcos Fernandez-Alfara², Veronica Chanes², Julia Carbo¹, Marta Ramirez-Pedraza¹, Oscar Reina², Louise Thingholm³, Corinna Bang³, Malte Rühlemann³, Andre Franke³, Robert Schierwagen⁴, Karl P. Rheinwald⁵, Jonel Trebicka⁴, Raul Mendez^{2,6}, Mercedes Fernandez^{1,*}

ABSTRACT

Objective: Obesity represents a growing health problem that is reaching pandemic dimensions and lacks effective cures, thus highlighting an urgent need for better mechanistic understanding and new therapeutic strategies. Unlike transcription, the function of translation in obesity has hardly been investigated. Here, we fill this knowledge gap by pinpointing a crucial function for gene regulation at the step of translation in diet-induced obesity.

Methods: We performed studies with human adipose tissue, high-fat-diet-induced obese mice and rats, CPEB4-knockout mice, and adipocyte lines. Cells were transfected with small-interfering RNAs that knockdown CPEB4. Transcriptome-wide identification and validation of CPEB4 targets in adipocytes were obtained by RNA-protein coimmunoprecipitation and high-throughput sequencing. The effect of CPEB4 depletion on high-fat-diet-induced dysbiosis was determined by 16S ribosomal-RNA gene sequencing and microbiome bioinformatics.

Results: We show that cytoplasmic polyadenylation element-binding protein 4 (CPEB4), which controls the translation of specific mRNAs by modulating their poly(A) tails, is highly expressed in visceral fat of obese but not lean humans and rodents (mice and rats), where it orchestrates an essential post-transcriptional reprogramming for aggravation of high-fat-diet-induced obesity. Mechanistically, CPEB4 overexpression in obese adipocytes activates the translation of factors essential for adipose tissue expansion (Cebpb, Stat5a) and adipocyte-intrinsic immune-like potential (Ccl2, Tlr4), as demonstrated by RNA-immunoprecipitation and high-throughput sequencing and experimentally validated in vivo. Consistently blocking CPEB4 production in knockout mice protects against diet-induced body weight gain and reduces adipose tissue enlargement and inflammation. In addition, the depletion of CPEB4 specifically in obese adipocytes using short hairpin RNAs decreases cell differentiation, lipid accumulation, and the proinflammatory and migratory capacity of macrophages. The absence of CPEB4 also attenuates high-fat diet-induced dysbiosis, shaping the microbiome composition toward a more beneficial profile, as shown by microbiome bioinformatics analysis.

Conclusion: Our study identifies CPEB4 as a driver and therapeutic target to combat obesity.

© 2021 The Author(s). Published by Elsevier GmbH. This is an open access article under the CC BY-NC-ND license (<http://creativecommons.org/licenses/by-nc-nd/4.0/>).

Keywords Obesity; Translation; RNA-Binding proteins; Adipose tissue; Microbiome dysbiosis

¹IDIBAPS Biomedical Research Institute, University of Barcelona, Barcelona, Spain ²Institute for Research in Biomedicine (IRB), The Barcelona Institute of Science and Technology, Barcelona, Spain ³Institute of Clinical Molecular Biology, Christian-Albrechts-University Kiel, University Hospital Schleswig Holstein Campus Kiel, Kiel, Germany ⁴Goethe University Frankfurt, Frankfurt, Germany ⁵Franziskus Krankenhaus, Cologne, Germany ⁶Institució Catalana de Recerca i Estudis Avançats (ICREA), Barcelona, Spain

*Corresponding author. Mercedes Fernandez, IDIBAPS Biomedical Research Institute, Rossello street 149-153, 08036 Barcelona, Spain. Tel.: +34 606 958606. E-mail: mercefernandez@ub.edu (M. Fernandez).

URL: <http://www.mercedesfernandezlab.com/>

Abbreviations: BMI, body mass index; CCL2, C–C motif chemokine ligand-2; C/EBP, CCAAT/enhancer binding protein; CPEB, cytoplasmic polyadenylation element binding protein; CSF1, colony stimulating factor-1; DAPI, 4,6-diamidino-2-phenylindole; FFA, free fatty acids; FMO, fluorescent minus one; GAPDH, glyceraldehyde 3-phosphate dehydrogenase; GLUT-4, glucose transporter type-4; GO, gene ontology; GSEA, gene set enrichment analysis; HFD, high fat diet; IL10, interleukin-10; IPTG, isopropyl β-D-1-thio-galactosidase; JAM-A, junctional adhesion molecule-A; KLF2, Krüppel like factor 2; mGWAS, microbiome genome-wide association studies; LBP, lipopolysaccharide-binding protein; MCP1, monocyte chemoattractant protein-1; NAFLD, nonalcoholic fatty liver disease; ND, normal diet; NEFA, non-esterified fatty acids; PCNA, proliferating cell nuclear antigen; PPAR-α, peroxisome proliferator-activated receptor-α; RIP-Seq, RNA-protein immunoprecipitation and high-throughput sequencing; shRNA, short hairpin RNA; STAT5A, signal transducer and activator of transcription 5A; TLR-4, Toll-like receptor-4; UCP-1, uncoupling protein-1; UTR, untranslated region; VEGF, vascular endothelial growth factor; WAT, white adipose tissue; ZO-1, zonula occludens-1

Received August 31, 2021 • Revision received October 26, 2021 • Accepted October 30, 2021 • Available online 10 November 2021

<https://doi.org/10.1016/j.molmet.2021.101388>

1. INTRODUCTION

Obesity is an increasingly prevalent public health problem associated with high morbidity and mortality. Its incidence is rising in epidemic proportions in adults and children, with an estimated two billion individuals affected worldwide [1]. This is particularly alarming because of the multiple obesity-associated pathologies and the lack of effective cures [2]. Accordingly, understanding the regulatory mechanisms of high-fat-diet-induced obesity to identify new druggable targets is of great importance to the health care community.

Alterations in gene expression regulation at the level of translation can have profound implications for obesity, but little is known about that since previous efforts focused mostly on transcription [1,2]. A critical mechanism of translational control is mediated by the cytoplasmic polyadenylation element binding (CPEB) proteins. In contrast to the general mechanism that accelerates translation, CPEB controls the translation of selected mRNAs that possess cytoplasmic polyadenylation elements (CPE) in their 3' untranslated region (UTR). The binding of CPEB to CPE allows elongation of the poly (A) tail to the 3' end of the mRNA and subsequent translation into protein [3–6]. Studies have reported that CPEB4 drives an aberrant post-transcriptional reprogramming in diseases such as cancer [7–9], liver disease [10–12], and neurodegenerative disorders [13]. Our team and other groups have also independently identified CPEB4 as a risk gene for obesity-related traits [14–19]. Accordingly, we herein investigated the impact of CPEB4 as a driving force behind the abnormal phenotype observed after persistent exposure to high-fat-diet feeding. Our findings strongly support that targeting CPEB4 may be a potential anti-obesity therapeutic strategy.

2. MATERIALS AND METHODS

2.1. Humans

Visceral white adipose tissue was obtained from abdominally obese patients ($n = 30$; mean age 42 ± 2 years; 73% women and 27% men) during bariatric surgery at the St. Franziskus-Hospital in Cologne, Germany. Obese subjects had a body mass index (BMI) > 40 kg/m². Some of the obese subjects ($n = 20$) also had excess fat accumulation in the liver or non-alcoholic fatty liver disease (NAFLD). All samples were snap-frozen in liquid nitrogen until protein extraction was performed. All subjects provided written informed and voluntary consent prior to enrollment in the study. This consent included an understanding that clinical information and biological samples would be used for research. The ethics committees of the North Rhine-Westphalian Chamber of Medicine (reference number 2017110) and of the University Hospital Bonn (reference number 194/17) approved this study. Samples from non-obese individuals (BMI < 25 kg/m²; $n = 10$; mean age 49 ± 4 years; women) having no evidence of liver disease or any other disease affecting visceral adipose tissue served as controls. These control samples were provided by the FATBANK platform promoted by the CIBEROBN and coordinated by the IDIBGI Biobank (Biobank IDIBGI, B.0000872), integrated into the Spanish National Biobanks Network. These samples were processed following standard operating procedures with the appropriate approvals by the Ethics, External Scientific and FATBANK Internal Scientific Committees.

2.2. Animals and diets

Male C57BL/6J mice or Sprague–Dawley rats (Charles River Laboratories International Inc., USA) were randomly divided into two groups: the normal diet group ND (mice: $n = 6$ –7/genotype; rats: $n = 18$) and the high-fat diet group (HFD) (mice: $n = 12$ –20/

genotype; rats: $n = 18$). The ND group was fed on a standard diet, including 7.42% fat, 17.49% protein, and 75.09% carbohydrate (Research Diets, USA). The HFD group was fed with a diet containing 60% fat, 20% protein, and 20% carbohydrate (D12492; Research Diets, USA). Mice and rats were fed *ad libitum* with free access to water for 16 weeks beginning at 6 weeks of age. Animal studies were performed according to procedures approved by the Institutional Animal Care and Use Committee (IACUC) protocols of the University of Barcelona and they complied with the National Institute of Health guidelines on the handling of experimental animals (NIH Publications No. 8023, revised 1978).

2.3. Lentivirus production and generation of stable CPEB4 knockdown adipocyte cell lines by inducible short hairpin RNAs

To generate CPEB4 knockdown adipocyte cell lines, short hairpin RNA (shRNA) encoding sequences were delivered to the 3T3-L1 cell line through lentiviral infection. Lentiviruses were produced by transfection of Human embryonic kidney 293 (HEK293) packaging cells with the plasmids psPAX2 (Addgene, Watertown, MA), pCMV-VSV-G (Addgene), and pLKOPuro-IPTG-3xLacO (Sigma), using the liposome-based DNA transfection reagent LipoD293 (SigmaGen, Rockville, MD). The inducible pLKO-Puro-IPTG-3xLacO vector carried a sequence-specific for CPEB4 shRNA expression (5'-GCTTGTAGGTGGCTTGGGGTG-3') or a scramble control sequence (5'-GCGCGATAGCGCTAATAATTT-3'). This vector contained a LacI (repressor) and a modified human U6 shRNA promoter with three LacO (operator) sequences, affording both tight regulation and great gene silencing. In the absence of isopropyl- β -D-1-thio-galactoside (IPTG), an analog of lactose, LacI binds to LacO preventing the expression of the shRNA. When IPTG is present, the allosteric LacI repressor changes conformation, releasing itself from LacO-modified human U6 promoter, subsequently allowing the expression of the shRNA. Media from transfected HEK293 cells were removed and replaced with fresh media every 24 h. At 72 h post-infection, media (containing the lentivirus but not the packaging cells) were harvested, filtered through a 0.22- μ m filter, and used to infect 3T3-L1 cells grown on 6-cm dishes. Efficiently transduced 3T3-L1 cells were selected with 4 μ g/ml puromycin to create stable CPEB4 knockdown 3T3-L1 cells inducible with 1 mM IPTG. Studies were further validated using a different shRNA sequence to knock down CPEB4 (5'-GCTGCGCATGGAGAGATAGA-3').

2.4. Flow cytometry

The stromal vascular fraction was isolated from mouse epididymal white adipose tissue, as described above. Cells resuspended in sorting buffer were counted using an automated cell counter, and pre-incubated with Fc Block (BD Biosciences) at the concentration of 1 μ g/10⁶ cell for 5 min at 4 °C, prior to staining with conjugated antibodies or their corresponding IgG controls for 30 min at 4 °C. This assures that any observed staining is due to the interaction of the antigen-binding portion of the antibody with an antigen on the cell surface. Antibodies used to identify macrophage subsets were BV-711 anti-mouse CD11c, eFluor 450 anti-F4/80 (clone BM8), PE-anti-CD206 (MMR) (clone MR6F3), and APC-CD11b (clone M1/70). Additionally, fluorescence minus one and single stain controls were carried out for all experiments in order to gate and compensate. After incubation with primary antibodies, cell suspensions were washed in 2 ml of sorting buffer and centrifuged at 500 *g* for 5 min. Cells at a concentration of 250,000 per condition were suspended in a 0.3 ml sorting buffer and analyzed by flow cytometry with a BD FACSDIVA5 cytometer system (BD Biosciences, San Jose, CA) and the data were analyzed using FACSDIVA v6.1.3 software. Live/Dead Near-IR (Thermo Fisher) was

used to exclude dead cells. Each sample was obtained from a pool of 5–7 mice (wild-type or CPEB4^{KO}).

2.5. Scratch wound-healing migration assay

Bone marrow-derived macrophages were isolated from mice, seeded onto silicone culture inserts (80,000 cells/insert; Ibidi GmbH, Planegg/Martinsried, Germany), and allowed to grow for 24h. Cells were then treated with 10 µg/µL mitomycin for 1h at 37 °C, and the inserts were carefully removed with sterile forceps. The medium was replaced with conditioned media from mature differentiated adipocytes, or with DMEM containing 10% FBS, and the dishes were incubated for 24h. Pictures of the wound scratch were obtained at the time of removal (time 0) and at 24h, using AxioCam MRC5 microscope camera (Zeiss, Göttingen, Germany). The macrophage cell migration rate in response to an adipocyte-derived extrinsic factor was quantified by counting the number of cells that had invaded the scratch at 24h, considering the reference area at time 0h. Experiments were performed in triplicate.

2.6. Transwell chamber migration assay

Chamber migration assays were performed using 0.47 cm² Transwell inserts with an 8 µm pore size membrane (#140629, Thermo Fisher Scientific). Conditioned media from adipocytes treated with free fatty acids for 24 h, medium containing 200 ng/ml CCL2 (Biolegend, San Diego, CA) as a positive control, or low-serum DMEM as negative control were placed in the lower chamber. One hundred thousand bone marrow-derived macrophages were suspended in the DMEM medium containing 0.1% serum and seeded in the upper part of the chamber. Cells were incubated at 37°C and 5% CO₂ for 3 h. Cells that had not migrated and remained in the upper chamber were removed by gently swiping the membrane with cotton tips. Cells that migrated were fixed with 2.5% glutaraldehyde, permeabilized with 0.5% Triton-X-100, and stained with 0.1% crystal violet. Images were taken using a DMR inverted microscope. Quantification of cell migration was conducted in six fields of 10x magnification/condition using a fluorescence microscope. Experiments were repeated 3–4 times.

2.7. Determination of adipocyte size

Tissue samples were collected, fixed in 10% neutral buffered formalin, embedded in paraffin, cut in 5-µm-thick sections, mounted on slides, and stained with hematoxylin & eosin, according to the standard protocols. To estimate adipocyte size in epididymal white adipose tissue, the digital NanoZoomer 2.0-HT slide scanner from Hamamatsu was used to digitalize the image. Images were then imported for computer-assisted quantitative image analysis using ImageJ software (version 1.34 s; National Institute of Health, USA). Pictures were converted into binary black and white images (8-bit; grey scale). The 'watershed' function was used to mark the boundaries of individual fat clumps. The 'analyze particle' command was used to determine clump numbers and areas with 'cellularity' set at 0.70–1 and 'size' set at 500-infinity. The command 'measure all' was used to automatically generate all measurements.

2.8. Statistical analysis

Data are shown as mean ± SEM. Results that were normally distributed ($P > 0.05$ from Kolmogorov–Smirnov test) were compared with parametric statistical procedures (two-tailed Student's t-test and ANOVA followed by Bonferroni's test for multiple comparisons). Non-normally distributed results were compared with non-parametric tests (Kruskal–Wallis one-way ANOVA and Mann–Whitney–U test). Statistical significance was accepted at $P < 0.05$. Sample sizes for reproducibility are indicated in the figure legends. Where

representative images for fluorescence staining, immunohistochemical staining, and immunoblot are shown, these results were independently observed at least three times. All in vitro experiments were repeated in at least three independent biological replicates. When possible, the investigators were blinded during experiments and outcome assessment.

3. RESULTS

3.1. CPEB4 expression is elevated in visceral white adipose tissue from obese patients and rodents

To elucidate the clinical relevance of CPEB4 in human obesity, we examined visceral white adipose tissue (WAT) specimens acquired from abdominally obese patients ($n = 30$; mean age 42 ± 2 years; 73% women and 27% men) during bariatric surgery at the St. Franziskus-Hospital in Cologne, Germany. Obese subjects had a body mass index (BMI) over 40 kg/m² (Figure 1A). Twenty obese subjects also had excess fat accumulation in the liver or non-alcoholic fatty liver disease (NAFLD). Samples from nonobese individuals (BMI < 25 kg/m²; $n = 10$; mean age 49 ± 4 years) having no evidence of liver disease or any other disease affecting visceral adipose tissue served as controls. Consistent with a potential role in human disease, expression of endogenous CPEB4 protein was higher in WAT from obese individuals, especially those with both obesity and liver steatosis (Figure 1B), compared to subjects with normal body weight. The upregulation of CPEB4 in WAT during obesity observed on protein level by immunoblotting was not confirmed on mRNA level, as measured by RT-PCR (Figure 1C), suggesting post-transcriptional regulation of CPEB4 overexpression in this context.

We also determined the expression of CPEB4 in intra-abdominal WAT of obese male Sprague–Dawley rats and C57BL/6J mice. To induce obesity, rodents were placed on a high-fat diet (HFD; 45% energy from fat in rats and 60% energy from fat in mice) or standard normal diet (ND; 13% energy from fat) over 16 weeks, starting at 6 weeks of age (Supplemental Fig. 1A). *Ad libitum* feeding of HFD in rats resulted in increased body weight and abdominal circumference (Supplemental Figs. 1B and C), and increased energy intake without differences in food intake (Supplemental Fig. 1D), compared with rodents fed ND. This was accompanied by insulin resistance (Supplemental Fig. 1E). In addition, visceral WAT, including epididymal, mesenteric, and retro-peritoneal WAT, was enlarged in HFD-fed rats (Supplemental Figs. 1F and G), both as absolute value and as a percentage of body mass versus animals fed ND, consistent with the development of obesity and confirming the obesogenic effect of HFD. Similar to the human studies, the expression of CPEB4 protein was increased in visceral WAT of rats (Supplemental Fig. 1H) and mice (Figure 1D) that were rendered obese by HFD consumption, compared to control animals fed ND. These findings suggest a pathophysiological role of CPEB4 regulating WAT in vivo. Mechanisms involved in the upregulation of CPEB4 signaling at the onset of obesity could include the increase in CPEB1 and Aurora kinase protein expression observed in WAT of HFD-fed animals (Supplemental Fig. 1H).

3.2. CPEB4 depletion reduces predisposition to diet-induced obesity

To dissect the contribution of CPEB4 to HFD-induced obesity, we generated a global loss-of-function genetic mouse model on a C57BL/6J background (CPEB4^{KO}). For comparison, we used littermates that retained the gene (denoted as wild-type controls). We confirmed successful ablation by the virtual absence of CPEB4 protein expression in WAT as compared to wild-type mice (Figure 1E). Six-week-old male

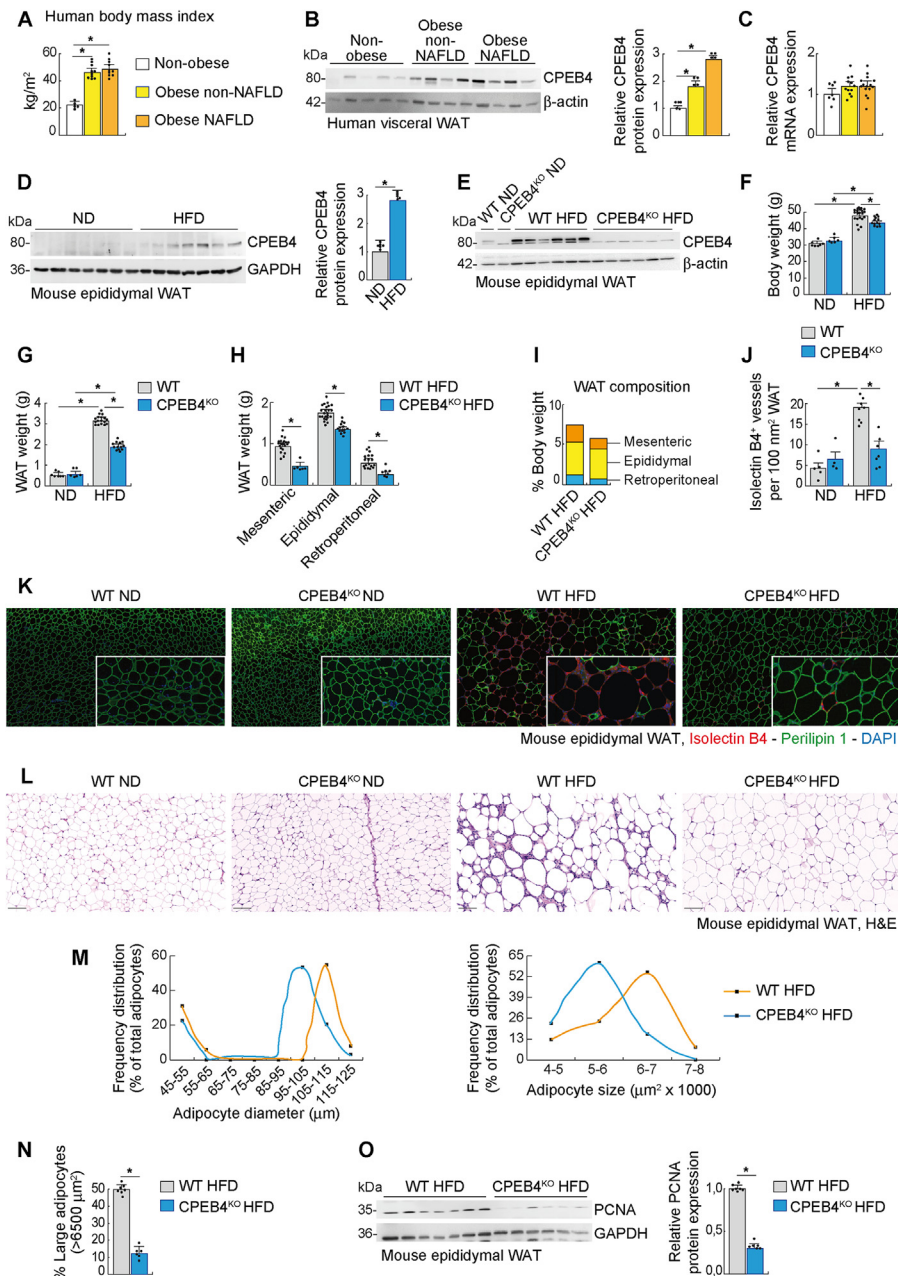


Figure 1: CPEB4 expression is elevated in obese human and rodent visceral adipose tissue, and CPEB4 depletion reduces predisposition to diet-induced obesity. (A)

Body mass index in human non-obese (BMI < 25 kg/m²; n = 10; mean age 49 ± 4 years; women) and obese (n = 30; mean age 42 ± 2 years; 73% women and 27% men) individuals. Few obese individuals presented non-alcoholic fatty liver disease (NAFLD) (n = 20). Non-obese individuals showed no evidence of liver disease or any other disease affecting visceral adipose tissue. **(B)** CPEB4 immunoblotting and protein expression quantification in visceral (omental) white adipose tissue (WAT) from a nonobese and obese human. β-Actin was used as a loading control. Unprocessed original images of blots are shown in [Supplemental Fig.6A](#). **(C)** CPEB4 mRNA expression in visceral WAT from nonobese (n = 7) and obese humans with (n = 13) or without (n = 14) NAFLD. **(D)** CPEB4 immunoblotting and protein expression quantification in epididymal WAT from mice on either normal diet (ND) or high-fat diet (HFD) for 16 weeks. GAPDH was used as a loading control. Unprocessed original images of blots are shown in [Supplemental Fig.6B](#). **(E)** CPEB4 immunoblotting and protein expression quantification in epididymal WAT from wild-type (WT) and CPEB4^{KO} mice fed HFD or ND. β-Actin was used as a loading control. Unprocessed original images of blots are shown in [Supplemental Fig.6C](#). Differences in the band pattern in different blots are due to different species, tissues, anti-CPEB4 antibodies used, or even batch-to-batch variations. In Fig.1E, the lower molecular weight band is a nonspecific band whereas the band on top, which disappears in CPEB4 knockout mice, corresponds to CPEB4. **(F)** Body weight in WT and CPEB4^{KO} mice fed with ND (n = 6–7/genotype) or HFD (n = 12–20/genotype). **(G)** Visceral WAT weight, in absolute amounts, calculated as the sum of weights of mesenteric, epididymal and retroperitoneal WAT from WT and CPEB4^{KO} mice fed with ND or HFD. **(H)** Absolute visceral fat weight of the different visceral fat depots in WT and CPEB4^{KO} mice after 16 weeks of HFD. **(I)** Percentage WAT composition of HFD-fed WT and CPEB4^{KO} mice. **(J)** Quantification of isolectin B4 positive vessels in epididymal WAT from WT and CPEB4^{KO} mice fed with ND (n = 4–5/genotype) or HFD (n = 6–8/genotype). **(K)** Representative images of co-immunofluorescence for isolectin B4 and perilipin-1 in epididymal WAT from WT and CPEB4^{KO} mice fed with ND or HFD. **(L)** Representative images of H&E-stained sections of epididymal WAT from WT and CPEB4^{KO} mice fed ND or HFD. Scale bar, 100 µm. **(M)** Frequency distribution of adipocyte diameter (left) and size (right) in epididymal WAT from HFD-fed WT (n = 7) and CPEB4^{KO} (n = 6) mice. **(N)** Percentage of large adipocytes in epididymal WAT from HFD-fed WT and CPEB4^{KO} mice. **(O)** PCNA immunoblotting and protein expression quantification in epididymal WAT from HFD-fed WT and CPEB4^{KO} mice. GAPDH was used as loading control. Unprocessed original images of blots are shown in [Supplemental Fig.6D](#). All values represent the mean ± SEM of independent biological replicates. *P < 0.05 (Student's t-test and ANOVA). See also [Supplemental Figs.1,2,6](#).

CPEB4^{KO} mice and age- and sex-matched wild-type littermates were fed *ad libitum* with either HFD (60% calories from fat; n = 12–20/genotype) or ND (13% calories from fat; n = 6–7/genotype) over 16 weeks (Supplemental Fig. 2A). CPEB4^{KO} mice on HFD did not gain as much weight as their wild-type counterparts on the same diet (Figure 1F, Supplemental Fig. 2B), indicating that knocking out CPEB4 reduces the predisposition to diet-induced obesity. On normal chow, body weight did not show a significant difference between CPEB4^{KO} and wild-type mice (Figure 1F, Supplemental Fig. 2B), consistent with the requirement of high-fat feeding for activation of the CPEB4 pathway. Both wild-type and CPEB4^{KO} mice displayed increased blood glucose levels after HFD feeding compared with the ND-fed groups, without differences between genotypes (Supplemental Fig. 2C). These results together suggest that the activation of CPEB4 signaling is associated with, and inactivation of CPEB4 conversely prevents HFD-induced excessive weight gain.

To ascertain whether the resistance of CPEB4^{KO} mice to gain body weight in response to HFD feeding reflects a specific decrease in visceral adiposity, we measured the weight of fat depots. Diet-induced obese mice lacking CPEB4 exhibited an overall reduction of the expansion of visceral WAT depots, whereas control mice did not. Thus, the size and absolute and relative weight (after normalization for total body weight) of the individual visceral adipose tissues (i.e., epididymal, mesenteric, and retroperitoneal) were significantly lower in HFD-fed CPEB4^{KO} mice than in wild-type mice on HFD (Figure 1G–I, Supplemental Figs. 2D–F). The decrease in adiposity in CPEB4^{KO} mice on HFD was paralleled by a reduction in the hypervascularity typically observed in obese adipose tissue [20], as demonstrated for the endothelial marker isolectin-B4 and the lipid droplet-associated protein perilipin-1 (Figure 1J–K), and immunoblotting for the proangiogenic vascular endothelial growth factor (VEGF) (Supplemental Fig. 2G).

Genetic ablation of CPEB4 in ND-fed mice, in which CPEB4 expression in WAT is low (Figure 1D,E), had no effect on adipose tissue weight, relative to wild-type littermates on the same diet (Figure 1G, Supplemental Figs. 2H–K), consistent with the lack of body weight differences and suggesting that CPEB4 is not required for visceral adipose tissue homeostasis in steady state. In addition, the anti-adipogenic effect of ablating CPEB4 was specific to WAT, since there were no differences in the weight of other organs, including the liver, spleen, small and large intestines, and brain (Supplemental Figs. 2L–O). These findings indicate that the reduced body weight of HFD-fed CPEB4^{KO} mice was largely accounted by a reduction in WAT weight.

Overall, these data support a critical functional role for CPEB4 in regulating adiposity *in vivo* under obesity conditions.

3.3. Loss of CPEB4 mitigates obesity-linked adipocyte hypertrophy

The observation that CPEB4^{KO} mice had reduced susceptibility to obesity prompted us to examine whether white adipocytes might rely on CPEB4-dependent reprogramming to fuel cell hypertrophy during excessive intake of fat calories. We noted that epididymal WAT from HFD-fed CPEB4^{KO} mice was characterized by the presence of smaller adipocytes compared to that from wild-type mice on the same HFD regimen (Figure 1L). Quantification of the frequency distribution by computerized image analysis revealed a shift in both adipocyte diameter and size in epididymal WAT from CPEB4^{KO} mice on HFD toward smaller cells relative to HFD-fed wild-type mice (Figure 1M). Accordingly, the proportion of large adipocytes, defined as having a surface area >6500 μm^2 , was significantly decreased in CPEB4^{KO} mice on HFD relative to wild-type animals on HFD (Figure 1N). We also observed a concomitant decrease in cellular proliferation in the

epididymal WAT of CPEB4^{KO} mice on the HFD than in wild-type mice on the same diet, as evidenced by immunoblotting for the proliferating cell nuclear antigen (PCNA) (Figure 1O). No cellular changes in the normal adipose tissue architecture, including changes in adipocyte size and number, were observed in CPEB4^{KO} mice compared to wild-type controls when both were on the ND (Supplemental Fig. 2P). These findings underscore the importance of CPEB4 in regulating adipocyte biology during obesity.

3.4. The absence of CPEB4 decreases obesity-associated adipocyte differentiation

To determine whether the attenuated expansion of visceral fat mass that we observed in HFD-fed CPEB4^{KO} mice was associated with a diminution of adipocyte differentiation, we used an *in vitro* approach in primary white adipocytes and a preadipocyte cell line. We isolated undifferentiated primary preadipocytes from fresh stromal vascular fractions of epididymal WAT of 4-month-old male mice (Figure 2A,B). To induce preadipocytes to differentiate into mature adipocytes, cells were treated with the adipogenic inducers fetal bovine serum (FBS), dexamethasone, isobutyl-methylxanthine, indomethacin, and insulin [21]. Thereafter, mRNA was extracted from both preadipocytes and mature adipocytes and performed quantitative PCR with reverse transcription (qRT-PCR) to determine the levels of mRNA encoding CPEB4. We found that CPEB4 mRNA, instead of other CPEB isoforms, was highly enriched in fully differentiated adipocytes compared to preadipocytes, as demonstrated by RT-PCR (Figure 2C). These results were validated in the 3T3-L1 mouse preadipocyte cell line, cultured under pro-differentiation conditions as described above for primary adipocytes. Thus, we observed that both mRNA (Figure 2D) and protein (Figure 2E) levels of CPEB4 were progressively increased throughout adipocyte differentiation, suggesting the process of overexpression of CPEB4 for adipocyte differentiation.

To functionally test for intrinsically altered white adipocyte differentiation potential after CPEB4 depletion, we depleted endogenous CPEB4 in 3T3-L1 adipocytes by transduction with recombinant lentiviruses expressing isopropyl- β -D-1-thio-galactoside (IPTG)-inducible short hairpin RNAs (shRNAs) targeting CPEB4 (CPEB4^{KD}). Control 3T3-L1 cells were transduced with scramble shRNAs or left untransduced; they were then induced to differentiation. Immunoblotting analysis of these cells demonstrated efficient silencing of CPEB4 by CPEB4 shRNAs (Figure 2F). Differentiating 3T3-L1 adipocytes lacking endogenous CPEB4 presented a severely compromised ability to form large, lipid-laden droplets characteristic of the mature fat cell phenotype, compared with control cells transduced with scramble shRNAs or left untransduced (Figure 2G), as demonstrated by Oil-Red O staining. Consistently, the incremental induction of the two principal adipogenic factors [21], peroxisome proliferator-activated receptor- γ (PPAR) and CCAAT/enhancer-binding protein (C/EBP α), was attenuated at mRNA (Figure 2H) and protein (Figure 2I,J) level in the CPEB4-deficient 3T3-L1 adipocytes during the differentiation process, relative to control cells. A reduction in the mRNA and protein expression of the glucose transporter type 4 (GLUT4) was also apparent in differentiating 3T3-L1 adipocytes depleted of CPEB4 (Figure 2H–J). These results were corroborated using a different shRNA sequence, which efficiently reduced CPEB4 expression and decreased differentiation in 3T3-L1 adipocytes (Supplementary Figs. 3A and B). These findings demonstrate that knockdown of CPEB4 reduced, in a cell-autonomous manner, the ability of primary adipocytes and 3T3-L1 adipocytes to undergo adipogenic differentiation and accumulate mature lipids. Notably, the loss of CPEB4 under HFD was associated with a strong tendency for lower lipolytic potential in fat cells under fed conditions,

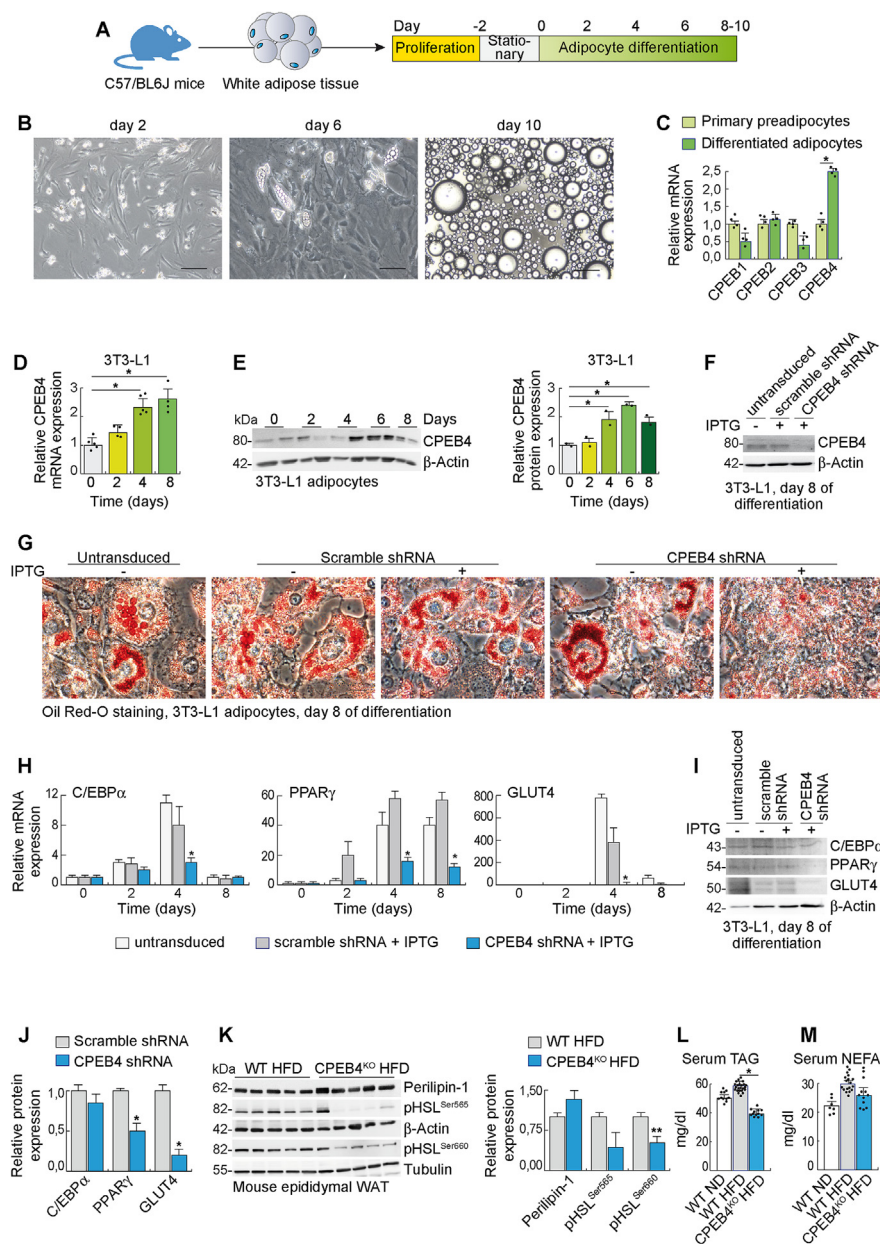


Figure 2: CPEB4 depletion decreases obesity-associated adipocyte differentiation. (A) Experimental set-up. Stromal vascular cells were isolated from mouse epididymal white adipose tissue, and then plated and grown to confluence. After 2 days of confluence (day 0), cells were induced to differentiate into mature adipocytes using the standard adipogenic medium. Two days post-induction, the medium was replaced with a maintenance medium, and cells were cultured for additional 8–10 days (see Materials and Methods for more details). (B) Representative phase-contrast micrographs of adipocytes isolated from mouse epididymal white adipose tissue. Scale bar, 100 μ m. (C) Expression of CPEB1, CPEB2, CPEB3 and CPEB4 mRNA in primary preadipocytes and differentiated primary adipocytes, isolated from mouse epididymal adipose tissue, measured by quantitative RT-PCR ($n = 3\text{--}4$ /cell type). (D) CPEB4 mRNA expression in 3T3-L1 adipocytes at different time points after inducing cell differentiation ($n = 4\text{--}5$ /time point). (E) CPEB4 immunoblotting and protein expression quantification in 3T3-L1 adipocytes at different time points after inducing cell differentiation. β -Actin was used as the loading control. Unprocessed original images of blots are shown in Supplemental Fig.6E. (F) CPEB4 immunoblotting in differentiated 3T3-L1 adipocytes, transduced with CPEB4 shRNA or scramble control shRNA, and treated with IPTG, or untransduced. Proteins were examined over three independent replicates per group. (G) Staining of cellular lipids by Oil Red O in 3T3-L1 adipocytes, transduced with scramble or CPEB4 shRNA, with or without IPTG, or untransduced. Lipid droplets are seen as pink/red vesicles. Studies were performed at day 8 of adipocyte differentiation ($n = 3$ independent experiments per group). Scale bar, 50 μ m. (H) Expression of the adipocyte differentiation markers C/EBP α , PPAR γ and GLUT4 mRNA in 3T3-L1 adipocytes at different time points after inducing cell differentiation ($n = 3$ independent biological replicates). (I) Immunoblotting for C/EBP α , PPAR γ and GLUT4 in 3T3-L1 adipocytes, transduced with scramble or CPEB4 shRNA, with or without IPTG, or untransduced. β -Actin was used as the loading control. Proteins were examined over three independent replicates per group. Unprocessed original images of blots are shown in fig.S5F–H. (J) Protein expression quantification of C/EBP α , PPAR γ , and GLUT4 in 3T3-L1 adipocytes, transduced with scramble or CPEB4 shRNA, with or without IPTG, or untransduced ($n = 3$ independent experiments). (K) Immunoblotting and protein expression quantification for the lipolysis markers perilipin-1 and HSL phosphorylated at Ser565 (pHSL^{Ser565}) or at Ser660 (pHSL^{Ser660}) in epididymal adipose tissue from HFD-fed WT and CPEB4^{KO} mice. α -Actin and tubulin were used as loading controls. Unprocessed original images of blots are shown in Supplemental Fig.6I,J. (L) Serum triglycerides (TAG) in HFD-fed WT and CPEB4^{KO} mice and ND-fed WT mice. (M) Serum non-esterified fatty acids (NEFA) in HFD-fed WT and CPEB4^{KO} mice and ND-fed WT mice ($n = 6\text{--}17$ /genotype/nutritional status). All values represent the mean \pm SEM of independent biological replicates. * $P < 0.05$ (Student's t-test and ANOVA). See also Supplemental Fig.3,6.

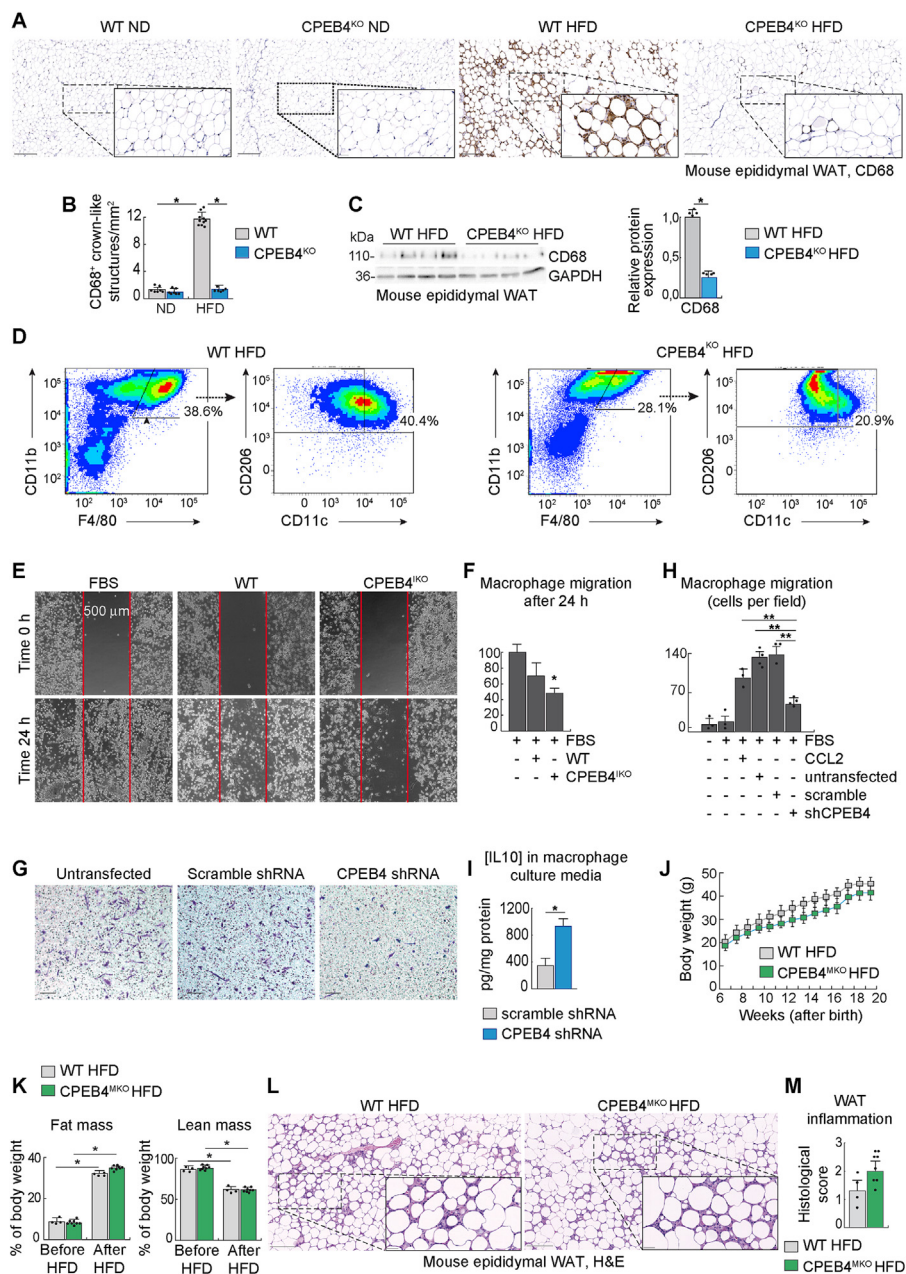


Figure 3: CPEB4 depletion decreases obesity-induced visceral adipose tissue inflammation. (A) Representative images of immunohistochemical staining for the macrophage marker CD68 in epididymal white adipose tissue (WAT) from WT mice fed ND or HFD, and HFD-fed CPEB4^{KO} mice. Higher-magnification images of the boxed regions are also shown. Scale bars, 100 μm. (B) Quantification of crown-like structures stained with antibodies against CD68 in epididymal WAT from WT and CPEB4^{KO} mice after being fed with HFD (n = 5–10/genotype) or ND (n = 6–7/genotype). (C) CD68 immunoblotting and protein expression quantification in epididymal WAT from HFD-fed WT and CPEB4^{KO} mice. GAPDH was used as the loading control. Unprocessed original images of blots are shown in Supplemental Fig. 6K. (D) Representative flow-cytometry plots showing frequencies of F4/80⁺CD11b⁺ macrophages among stromal vascular cells isolated from epididymal WAT of HFD-fed WT or CPEB4^{KO} mice (n = 5–7), as well as frequencies of CD11c⁺CD206⁺ macrophages among F4/80⁺CD11b⁺ cells. See controls in fig.SB-D. (E) Scratch wound-healing cell migration assay. Bone marrow-derived macrophages isolated from wild-type (WT) mice were treated with conditioned medium from adipocytes isolated from WT mice or tamoxifen-inducible CPEB4 knockout mice (CPEB4^{KO}). See experimental set-up in Supplemental Fig. 4H. (F) Quantification of macrophage migration from scratch cell migration assays described in (E) (n = 3 independent biological replicates). The number of cells that had invaded the scratch at 24h was counted, considering the reference area at time 0h. (G) Transwell chamber cell migration assay showing that migration of macrophages is inhibited by conditioned media derived from CPEB4 shRNA-transduced adipocytes, compared with macrophages exposed to conditioned media from scramble shRNA-transduced or untransduced adipocytes. Scale bar, 100 μm. See experimental set-up and additional controls in Supplemental Fig. 4I. (H) Quantification of macrophage migration from transwell cell migration assays described in (G) (n = 3–4 independent biological replicates). (I) The concentration of the anti-inflammatory cytokine IL10 in macrophages exposed to conditioned media from scramble shRNA-transduced or CPEB4 shRNA-transduced adipocytes, treated with free fatty acids for 24h (n = 3 independent biological replicates). (J) Bodyweight change during 14 weeks of HFD in WT (n = 6) and myeloid-specific CPEB4^{MKO} mice (n = 10). (K) Body fat mass (left) and lean mass (right) measured by magnetic resonance imaging in WT and myeloid-specific CPEB4^{MKO} mice after 14 weeks of HFD. (L) H&E-stained sections of epididymal WAT in myeloid-specific CPEB4^{MKO} knockout mice. Scale bar, 250 μm. Higher-magnification images of the boxed regions are also shown. (M) Histological score of epididymal WAT inflammation in myeloid-specific CPEB4^{MKO} knockout mice. All values represent the mean ± SEM of independent biological replicates. *P < 0.05, **P < 0.01 (Student's t-test and ANOVA). See also Supplemental Fig. 4, 6.

as reflected by upregulation of perilipin-1 and downregulation of phosphorylated hormone-sensitive lipase (pHSL) (Figure 2K), strengthening the idea that limited WAT differentiation and adipogenic capacity rather than increased lipolysis are the main contributors to the decreased visceral adiposity observed in CPEB4^{KO} mice under HFD. Therefore, HFD-fed CPEB4^{KO} mice also exhibited reduced serum triglyceride levels (Figure 2L), whereas serum concentrations of non-esterified fatty acids (NEFA) showed no significant elevation (Figure 2M), compared with HFD-fed wild-type mice. These observations, together with the presence of CPEB4 in the stromal-vascular fraction of WAT and the upregulation of CPEB4 during adipocyte differentiation, are indicative of a restricted capacity of CPEB4-deficient preadipocytes to differentiate into mature fat cells and may explain the reduced adiposity of the HFD-fed CPEB4^{KO} mice. Furthermore, CPEB4 depletion did not significantly modify the expression of the uncoupling protein 1 (UCP1) in obese retroperitoneal or epididymal WAT from HFD-fed mice (Supplementary Figs. 3C–F), suggesting that the reduction in body weight gain observed after HFD feeding in the absence of CPEB4 was not attributable to alterations in thermogenesis.

3.5. Ablation of CPEB4 reduces obesity-induced white adipose tissue inflammation

The expansion of adipocytes during the development of obesity gives rise to unhealthy adipose tissue, characterized by low-grade inflammation and the accumulation of proinflammatory macrophages [22]. This finding was supported wild-type mice following prolonged high-fat feeding (Figure 3A,B, Supplemental Fig. 4A). This obesity-induced proinflammatory profile within abdominal fat depots was markedly diminished by CPEB4 depletion. Thus, the formation of crown-like structures by CD68⁺ macrophages (Figure 3A,B, Supplemental Fig. 4A) and CD68 protein expression (Figure 3C) were greatly reduced in epididymal WAT of HFD-fed CPEB4^{KO} mice, compared to HFD-fed wild-type mice. To define changes in macrophage populations, we isolated the epididymal stromal vascular fraction of wild-type and CPEB4^{KO} mice fed with HFD or ND for 16 weeks and performed flow cytometry analysis using the appropriate panel of fluorescent-conjugated antibodies (Figure 3D, Supplemental Fig. 4B). To minimize the impact of the intrinsic autofluorescence of adipose tissue macrophages, we carefully selected the fluorochromes for each cell marker and used fluorescent-minus-one controls (FMOs) (Supplementary Figs. 4C and D). Upon prolonged HFD feeding, an F4/80⁺CD11b⁺ double-positive population of macrophages, containing the majority of WAT macrophages and poorly represented in animals fed a normal diet (Supplemental Fig. 4C), surged in the epididymal WAT of wild-type mice (Figure 3D). Ablation of CPEB4 markedly reduced the percentage of this F4/80⁺CD11b⁺ total adipose tissue macrophage population (Figure 3D), consistent with the reduction in WAT inflammation observed in CPEB4^{KO} mice during diet-induced obesity.

Additionally, we performed further subfractionation of the purified F4/80⁺CD11b⁺ macrophage population of epididymal WAT, using the CD206 and CD11c markers. Targeted ablation of CPEB4 in an obesity setting altered the activation status of the WAT macrophages such that they were prominently anti-inflammatory, in concordance with the observation that CPEB4 deletion prevents the generation of low-grade inflammation in response to high-fat feeding. Thus, elimination of CPEB4 protein in HFD-fed mice was found increased the proportion of the pro-resolving F4/80⁺CD11b⁺CD206⁺CD11c⁻ macrophage subtype, which characteristically populates lean WAT and secretes anti-inflammatory cytokines to maintain homeostasis, and decreased the content of proinflammatory F4/80⁺CD11b⁺CD206⁻CD11c⁺

macrophages, which typically accumulate in the obese WAT and release inflammatory factors that impair homeostasis [22], compared to HFD-fed control mice retaining CPEB4 (Figure 3D). These results support the idea that dysregulation of CPEB4 expression in obese WAT is causally linked to obesity-associated WAT inflammation.

3.6. Depletion of CPEB4 reduces the production of chemotactic and proinflammatory factors by adipocytes, leading to diminished macrophage inflammatory activation and migration

To mechanistically explore the causal relationship between adipocyte CPEB4 expression and macrophage activation in obesity, we conducted loss-of-function studies in vitro. We initially knocked CPEB4 down in mouse 3T3-L1 preadipocytes via transduction with recombinant lentiviruses expressing IPTG-inducible short hairpin RNAs (shRNAs) against CPEB4 (CPEB4^{KD}) (Supplemental Fig. 4E). These CPEB4-depleted preadipocytes were induced to differentiate into mature 3T3-L1 adipocytes for 10 days; then exposed to free fatty acids (FFA; palmitic, oleic, and linoleic acids, which are abundant in obese WAT) for up to 24 h, to mimic the in vivo context of high-fat feeding and WAT inflammation. We harvested cell-free conditioned medium from these mature adipocytes post-stimulation and used it to treat primary mouse bone marrow-derived macrophages isolated from wild-type mice and placed in functional scratch migration assays with Ibidi silicone inserts. As controls, macrophages were incubated with conditioned media from 3T3-L1 adipocytes transduced with scramble shRNAs with or without IPTG, transduced with CPEB4 shRNA without IPTG, or left untransduced. This in vitro system models the pathophysiology of obesity-related WAT inflammation where most of the WAT macrophages are derived from bone marrow. The migratory properties of macrophages were significantly impaired when exposed to conditioned media from CPEB4^{KD} adipocytes (Supplementary Figs. 4F and G), which is consistent with a role for CPEB4 inducing the production of adipocyte-derived factors that paracrinally promote macrophage migration during obesity.

To investigate whether this reduced macrophage migratory capacity induced by CPEB4 silencing in adipocytes was mediated by a direct effect of CPEB4 on mature adipocytes and not by the observed effect of CPEB4 on adipogenesis (Figure 1L–N), and differentiation (Figure 2G–J), we generated mice with tamoxifen-inducible CPEB4 deletion (CPEB4^{IKO}) (Supplemental Fig. 4H). Stromal vascular fraction preadipocytes were isolated and cultured from the epididymal WAT of these mice. Mouse primary preadipocytes were subjected to differentiation and then stimulation with FFAs. Differentiated, mature adipocytes were then exposed to 1 μM tamoxifen to induce depletion of CPEB4. Control adipocytes retaining CPEB4 expression were exposed to the vehicle. The adipocyte-conditioned Medium was collected and used to treat bone marrow-derived macrophages obtained from wild-type mice and measure their migration. Notably, macrophages exposed to conditioned medium derived from CPEB4^{IKO} adipocytes exhibited less migration capability than did macrophages exposed to conditioned medium derived from control wild-type adipocytes (Figure 3E,F), strongly indicating that this effect was a CPEB4-mediated cell-autonomous effect on the already mature adipocyte and suggesting that this function is largely linked to the anti-inflammatory properties of CPEB4-depleted adipocytes rather than merely due to a defect in differentiation.

To explore this further, we analyzed the ability of macrophages to directionally respond to chemoattractants released by adipocytes. We designed cell migration Transwell assays where conditioned medium from adipocytes was placed into the lower part of a chamber and bone marrow-derived macrophages were seeded in the upper chamber

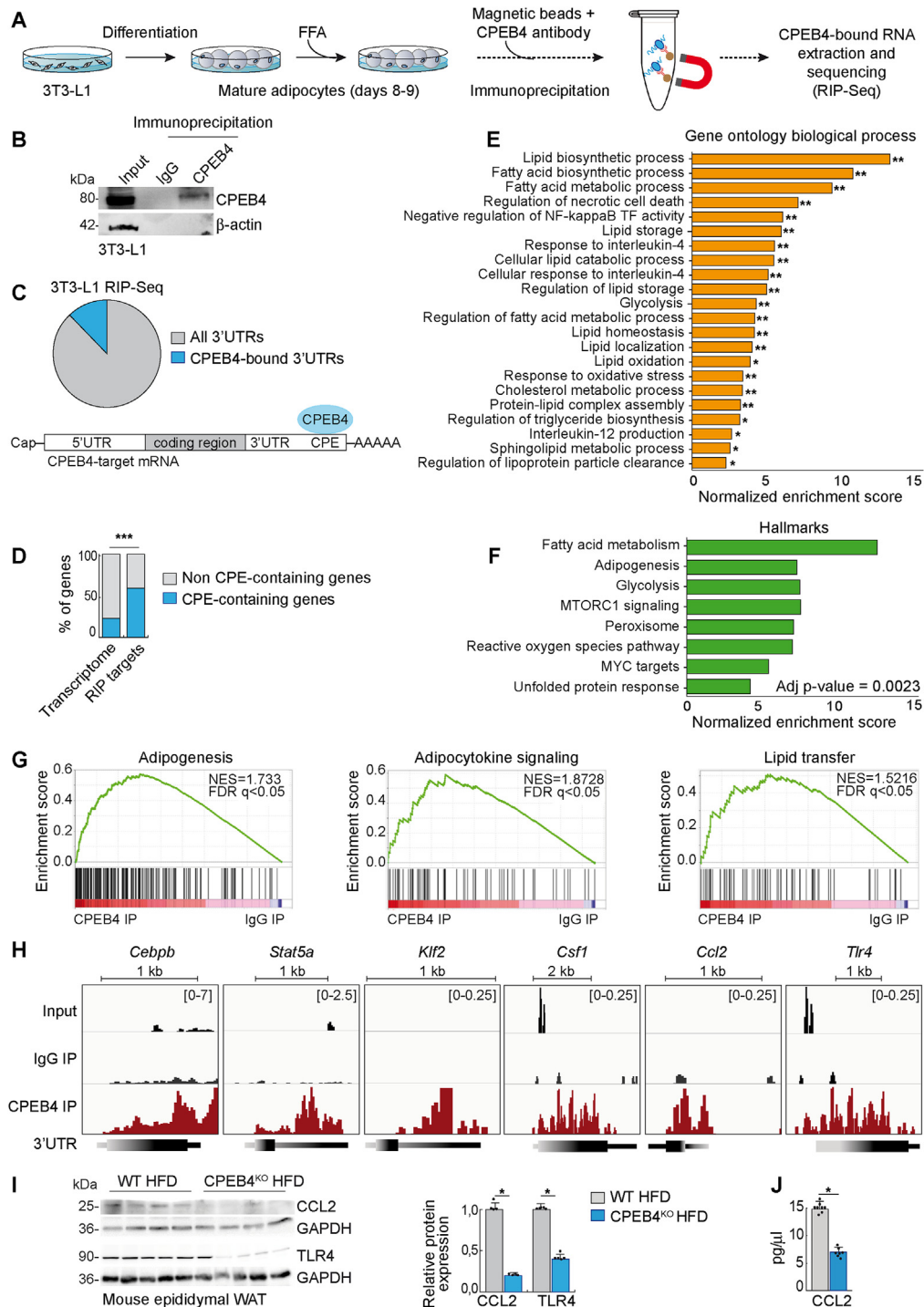


Figure 4: Identification of CPEB4 targets in adipocytes. (A) Schematic representation of our RIP-seq approach to identify CPEB4 targets in mature and free fatty acids (FFA)-treated 3T3-L1 adipocytes. (B) The efficiency of CPEB4 immunoprecipitation in adipocytes. Immunoprecipitations with nonspecific IgG were carried in parallel as a control. (C) CPEB4 targets were defined as those significantly enriched in wild-type CPEB4 immunoprecipitation, compared to the corresponding IgG immunoprecipitation ($FC_{(IP/Input)/(IgG/Input)} > 1.5$ and $P\text{-value} < 0.05$). (D) Percentage of genes with (+CPEs) or without (-CPEs) cytoplasmic polyadenylation element motifs in their 3'UTRs, comparing RIP targets versus the mouse transcriptome. Fisher's test $P\text{-value} < 2.2 \times 10^{-16}$. (E) Top Gene Ontology biological process categories enriched in CPEB4 targets in 3T3-L1 adipocytes treated with free fatty acids during 24h. Representations of the normalized enrichment score with adjusted $P\text{-value}$ of 0.0023 using Benjamini statistics. (F) Normalized enrichment score of hallmark 3'UTR sets (Broad Institute) upregulated in CPEB4 immunoprecipitation versus Input immunoprecipitation. Categories with the highest enrichment scores are depicted. (G) Gene Set Enrichment Analysis (GSEA). NES, normalized enrichment score. FDR, false discovery rate. (H) Read coverage of *Cebpb*, *Stat5a*, *Klf2*, *Csf1*, *Ccl2* and *Tlr4* mRNAs in RNAseq (Input) or RIP-seq samples (IPs). Detected peak enrichments in CPEB4 IP versus IgG IP are shown. Image obtained using integrated genomic viewer with a minimum range of 0–0.25 Reads per Million (RPM). (I) Immunoblotting and protein expression quantification for CCL2 and TLR4 in epididymal WAT from HFD-fed wild-type (WT) or CPEB4^{KO} mice. GAPDH was used as loading control. Unprocessed original images of blots are shown in Supplemental Fig.6L,7A. (J) CCL2 protein levels, determined by ELISA, in epididymal WAT tissue from HFD-fed WT ($n = 8$) or CPEB4^{KO} mice ($n = 7$). All values represent the mean \pm SEM of independent biological replicates. * $P < 0.05$, ** $P < 0.01$ (Student's $t\text{-test}$). See also Supplemental Fig.6,7.

(Supplemental Fig. 4I). We observed that conditioned medium from wild-type adipocytes (untransduced or transduced with scramble shRNA) increased macrophage migration, which was even greater than the migration elicited by the well-known chemotactic C–C motif chemokine ligand-2 (CCL2) (also referred to as monocyte chemoattractant protein-1) [23] (Figure 3G,H, Supplemental Fig. 4J). This migratory ability was severely reduced in macrophages treated with conditioned medium from adipocytes lacking CPEB4 (i.e., transduced with CPEB4 shRNA) (Figure 3G,H), indicating that the CPEB4-dependent release of factor(s) from adipocytes triggered macrophage migration. Macrophages exposed to conditioned media from FFA-treated CPEB4 shRNA-transduced adipocytes released higher levels of IL-10 (Figure 3I), an anti-inflammatory cytokine [24], compared with macrophages exposed to conditioned media from adipocytes transduced with scramble shRNA. These results collectively suggest that differentiated obese adipocytes, which express high levels of CPEB4, generate and release factors that drive at least part of the migratory and inflammatory phenotype of adipose macrophages, in a critical process that is CPEB4-dependent since adipocytes lacking CPEB4 do not have this capacity.

Furthermore, myeloid-specific CPEB4 deficiency did not affect obesity or visceral adipose inflammation. Thus, we used myeloid cell-specific CPEB4 knockout mice (CPEB4^{MKO}) generated by crossing CPEB4^{lox/lox} mice with transgenic mice expressing Cre-recombinase under the control of the lysozyme 2 gene (*Lyz2*) promoter. Wild-type CPEB4^{+/+} + Cre^{T/+} littermates were used as controls. We found that mice lacking CPEB4 exclusively in myeloid cells, when placed on HFD, showed no difference in body weight gain (Figure 3J), growth of visceral WAT (Figure 3K, Supplemental Figs. 4K and L), and visceral WAT inflammation (Figure 3L, M), as compared to wild-type mice on the same diet. Therefore, we consider it unlikely that the anti-adipogenic and anti-inflammatory effects observed in the whole-body CPEB4^{KO} mice on HFD were attributed to the deletion of CPEB4 in macrophages or myeloid cells.

3.7. High-throughput sequencing identification of CPEB4 targets in adipocytes reveals factors involved in adipogenesis and macrophage chemoattraction

To identify CPEB4 mRNA targets in adipocytes in an unbiased, transcriptome-wide manner, we performed RNA-protein immunoprecipitation in differentiated and FFA-treated 3T3-L1 cells with either CPEB4-specific antibody or anti-IgG antibody (as negative control) and sequenced the RNA recovered from the immunocomplexes by high-throughput sequencing (RIP-Seq) (Figure 4A). The efficiency of the CPEB4 immunoprecipitation was compared to the immunoprecipitation with nonspecific IgG carried in parallel as control (Figure 4B). Because CPEB4 activates the translation of genes by binding to specific CPE sequences located in the 3' untranslated region (3'UTR) of their mRNAs (Figure 4C), we measured overall RIP 3'UTR signal enrichment in CPEB4 versus input RIP samples (DeSeq2, BH-p-value < 0.05, FC > 1.5). This analysis revealed that 2767 different mRNAs were bound to CPEB4, representing 12% of the total 3'UTRs obtained in the transcriptome analysis of adipocytes (Figure 4C). Consistently, when running the CPE-prediction algorithm [6], the dataset was highly enriched in genes containing CPE motifs in their 3'UTRs, as expected of CPEB4 targets, compared to the whole transcriptome (Figure 4D). Candidates were then adjusted by performing an interaction analysis (IP/Input vs IgG/Input) which resulted in a reduced list of 246 strong CPEB4 mRNA targets (Supplemental Table 1). As a quality control, previously described CPEB4 targets such as vascular endothelial

growth factor A (VEGFA) were identified, while GAPDH as a negative control could not be identified.

To determine the functions of the protein-coding mRNAs that are significantly bound by CPEB4 in adipocytes, bioinformatics experts of our team conducted Gene Ontology (GO) analysis, Hallmark Enrichment scores (Broad Institute), and Gene Set Enrichment Analysis (GSEA). These analyses showed that adipocyte CPEB4 preferentially binds mRNAs involved in lipid metabolism, adipogenesis, adipocytokine signaling pathway, and the adipocyte-intrinsic immune-like potential (Figure 4E,F). Among CPEB4-regulated mRNAs, we identified several factors involved in adipocyte development [21], such as the CCAAT/enhancer-binding protein beta (*Cebpb*), the signal transducer and activator of transcription 5A (*Stat5a*) or the Krüppel-like factor-2 (*Klf2*) (Figure 4G), which is consistent with the phenotype unveiled in our present work where preadipocytes without CPEB4 were unable to undergo differentiation. Importantly, these CPEB4-regulated mRNAs may be required to maintain the differentiated phenotype of the mature adipocyte after adipogenesis and maturation. The RIP-seq analysis also highlighted the necessity of CPEB4 for the production of adipocyte-derived proinflammatory adipokines and factors essential for activation and recruitment of proinflammatory macrophages into obese fat depots [22,24,25], such as the monocyte chemoattractant protein-1 (*Ccl2* or *Mcp1*), the Toll-like receptor-4 (*Tlr4*) and the colony-stimulating factor-1 (*Csf1*) (Figure 4G).

To validate CPEB4 regulation of selected targets, we focused on CCL2 and TLR4 because they have been shown to play a unique and central role in attracting macrophages into obese adipose tissue [23,25]. The protein expression of CCL2 and TLR4 was significantly attenuated in vivo after CPEB4 depletion in CPEB4^{KO} mice fed with HFD (Figure 4H), compared with HFD-fed wild-type mice, as assessed by immunoblotting. CCL2 protein levels, determined by ELISA, were also reduced in epididymal WAT tissue from HFD-fed CPEB4^{KO} mice (Figure 4I), compared with HFD-fed wild-type mice. Altogether these results indicate that CPEB4 drives a post-transcriptional reprogramming in obese adipocytes that regulate the function of fat cells and their proinflammatory profile.

3.8. The absence of CPEB4 attenuates HFD-induced dysbiosis, shaping the microbiome composition towards a more beneficial profile

Recent studies from our team members and others demonstrate that dietary fat and obesity in humans and mice majorly impact gut microbiota composition and vice versa [26,27]. The causal, and not merely correlational, relationship between microbial dysbiosis and obesity-associated adipose tissue dysfunction and inflammation is increasingly recognized [27,28]. Importantly, we have also recently found that in large-scale microbiome genome-wide association studies (mGWAS) in humans, the locus harboring the CPEB4 gene on chromosome 5 is associated with variations in microbiota composition [29,30]. We and other groups have also previously reported the association of this locus with obesity-related traits [14–19]. Given this feature of microbiota composition dependence on CPEB4 and the role of HFD-induced dysbiosis amplifying the obesity-associated pathogenicity, we next examined the effects of CPEB4 ablation on the alterations in gut bacterial composition induced by consumption of a diet rich in fat. To this end, we collected caecal luminal fecal content, as a surrogate for the intestinal microbial content, from CPEB4^{KO} and wild-type littermates fed the same high-fat diet over sixteen weeks and housed in the same animal facility. These stool samples were subjected to the high-throughput method of 16S ribosomal RNA gene

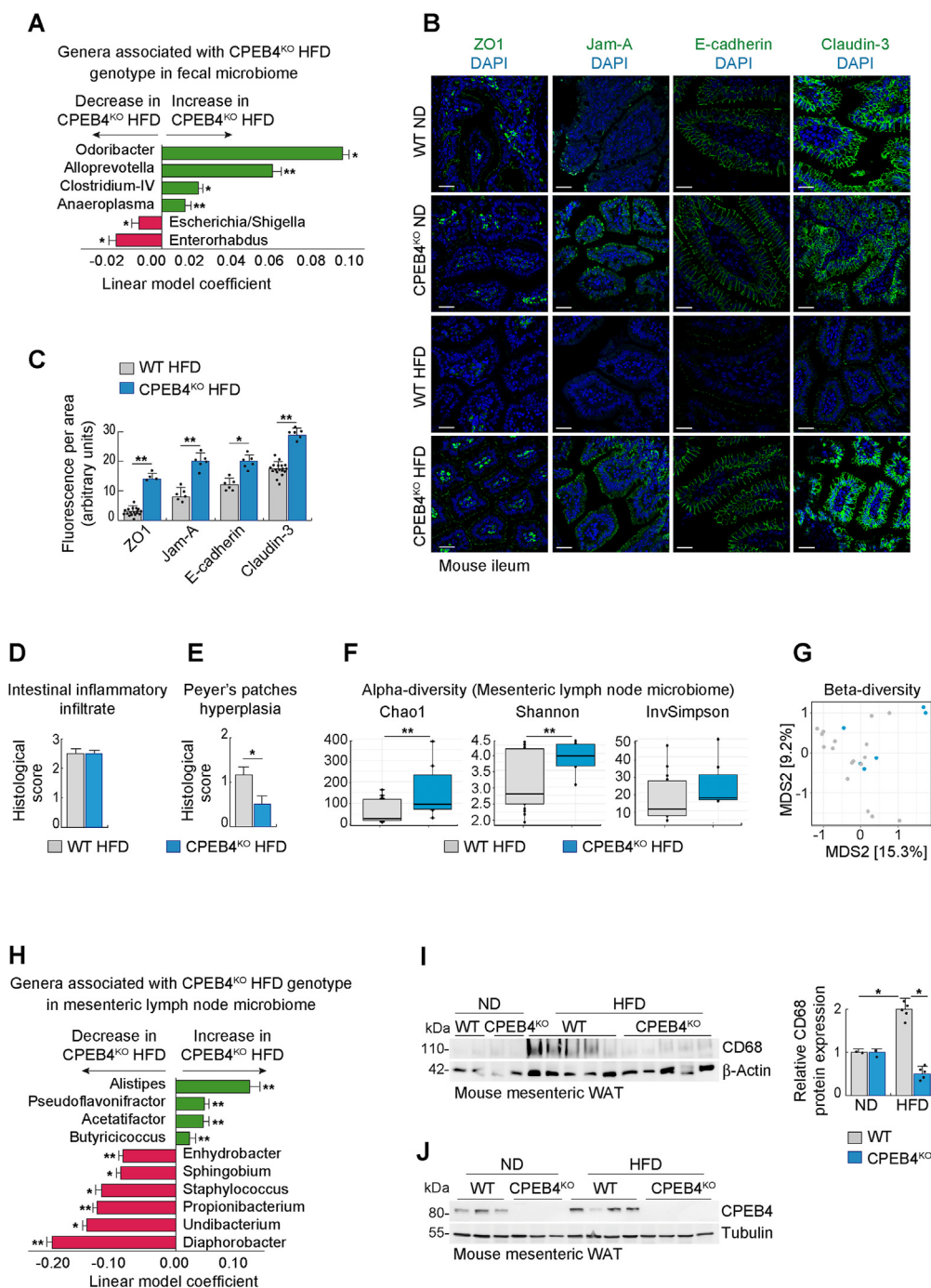


Figure 5: CPEB4 depletion attenuates obesity-associated dysbiosis. (A) Linear model coefficient from HFD-fed CPEB4^{KO} (n = 6) and wild-type (n = 16) mice. Fecal content was aseptically collected from mice and subjected to DNA extraction and 16S rRNA gene sequencing. Ordination plots were generated using the phyloseq function plot_ordination and ordinate with method CAP, Bray-Curtis dissimilarity and conditioned on the cage. (B) Representative confocal images of ZO1, Jam-A, E-cadherin and claudin-3 in the ileum of WT and CPEB4^{KO} mice fed ND or HFD. Nuclei were stained with DAPI (blue). Scale bar, 50 μ m. (C) Quantification of immunofluorescences of ZO1, Jam-A, E-cadherin, and claudin-3 in the ileum of HFD-fed WT (n = 6–18) and CPEB4^{KO} (n = 6) mice. (D) Histological score of intestinal (ileum) inflammatory infiltrate (score: 0, absence; 1, minimum; 2, slight; 3, moderate; 4, marked; 5, severe). Analyses were carried out by board-certified anatomic pathologists at IRB. (E) Histological score of Peyer's patches hyperplasia. Analyses were carried out by board-certified anatomic pathologists at IRB. (F) Alpha-diversity in mesenteric lymph node microbiome from HFD-fed CPEB4^{KO} (n = 6) and wild-type (n = 17) mice. (G) Beta-diversity in mesenteric lymph node microbiome from HFD-fed CPEB4^{KO} (n = 6) and wild-type (n = 17) mice; P = 0.041. (H) Linear model coefficient in mesenteric lymph node microbiome from HFD-fed CPEB4^{KO} (n = 6) and wild-type (n = 17) mice. Mesenteric lymph nodes were aseptically collected from mice and subjected to DNA extraction and 16S rRNA gene sequencing. Ordination plots were generated using the phyloseq function plot_ordination and ordinate with method CAP, Bray-Curtis dissimilarity, and conditioned on the cage. (I) CD68 immunoblotting and protein expression quantification in the mesenteric white adipose tissue (WAT) of WT and CPEB4^{KO} mice fed an ND or HFD. β -Actin was used as the loading control. Unprocessed original images of blots are shown in Supplemental Fig.7B. (J) CPEB4 immunoblotting and protein expression quantification in the mesenteric WAT of WT and CPEB4^{KO} mice fed a ND or HFD. Tubulin was used as loading control. Unprocessed original images of blots are shown in Supplemental Fig. 7. All values represent the mean \pm SEM of independent biological replicates. *P < 0.05, **P < 0.01 (Student's t-test). See also Supplemental Fig. 5,7.

sequencing to identify the specific phylogenetic profiles associated with the depletion of CPEB4 in mice maintained on HFD. This culture-independent method has significantly advanced our knowledge of gastrointestinal flora compared with conventional culture methods considering that up to 70–80% of intestinal bacteria are unculturable [31]. We found that the absence of CPEB4 had a significant impact on the HFD-induced abnormal microbiome, shaping its composition toward a more beneficial profile (Figure 5A), without meaningful changes in diversity (Supplemental Figs. 5A and B). Thus, compared to HFD-fed wild-type mice, the fecal microbiota composition of HFD-fed CPEB4^{KO} mice had a significantly higher relative abundance of butyrate-producing bacteria genera with anti-inflammatory properties [31], such as *Odoribacter*, *Alloprevotella*, *Clostridium-IV*, and *Anaeroplasm*, and a lower proportion of lipopolysaccharide-containing proinflammatory bacteria belonging to the genera *Escherichia/Shigella* and *Enterorhabdus* (Figure 5A), which are generally considered pathogenic [32,33].

We further investigated the effect of CPEB4 depletion on tight junction assembly following HFD feeding. The rationale is that prolonged high fat intake and obesity have previously been reported to disrupt the intestinal epithelial barrier integrity in both humans and rodents via a reduction in intercellular junctions among epithelial cells, alterations that may be at least partly explained by HFD-induced dysbiosis [34]. Immunofluorescence analysis revealed that the expression of the intestinal epithelial tight junction proteins zonula occludens-1 (ZO-1), junctional adhesion molecule A (JAM-A), E-cadherin, and claudin-3 was higher in the ileum of HFD-fed CPEB4^{KO} mice than in wild-type littermates (Figure 5B,C; Supplemental Figs. 5C and D), suggesting that the intestinal epithelial barrier is less vulnerable to HFD in the absence of CPEB4.

The coexistence of compromised barrier integrity and dysfunctional microbiome in obesity (with reciprocal aggravation) could facilitate the trafficking of enteric bacteria from the intestinal lumen into the contiguous mesenteric fat and mesenteric lymph nodes, the first organ encountered in the translocation route from the gastrointestinal tract [35]. Therefore, we hypothesized that the improvement of gut barrier function and microbiota composition upon elimination of CPEB4 after fat consumption may impact bacterial translocation, thereby influencing inflammation in mesenteric adipose tissue. We found that loss of CPEB4 in HFD-fed mice had no observable effects on ileal inflammation (Figure 5D), though it markedly attenuated the hyperplasia of intestinal Peyer's patches, a gut-associated lymphoid tissue connected to mesenteric lymph nodes (Figure 5E), as demonstrated by histological analyses carried out by board-certified anatomic pathologists at IRB. Importantly, using next-generation sequencing of the bacterial 16S rRNA gene, we also found that mesenteric lymph nodes from HFD-fed CPEB4^{KO} mice had a distinctly different microbial profile to that observed in HFD-fed wild-type mice (Figure 5F–H). Thus, in the absence of CPEB4, the mesenteric lymph node microbiome of HFD-fed mice had increased diversity (Figure 5F,G), the selective overabundance of the anti-inflammatory butyrate-producing bacteria *Alistipes*, *Pseudoflavonifractor*, *Acetatifactor*, and *Butyricoccus*, and reduced relative prevalence of the proinflammatory and harmful bacteria *Enhydrobacter*, *Sphingobium*, *Staphylococcus*, *Propionibacterium*, *Undibacterium*, and *Diaphorobacter* (Figure 5H), compared with HFD-fed wild-type mice. Mesenteric lymph nodes of HFD-fed CPEB4^{KO} mice host bacterial types that may trigger less aggressive inflammatory responses than those of HFD-fed wild-type mice. This possibility is supported by the substantial decrease in inflammation observed in the mesenteric adipose tissue of CPEB4^{KO} mice on HFD (Figure 5I,J),

compared with wild-type mice on the same diet. Effective depletion of CPEB4 in mesenteric adipose tissue of CPEB4^{KO} mice is shown in Figure 5J.

3.9. CPEB4 depletion decreases the susceptibility to obesity-related liver inflammation

The liver is one of the most exposed organs to bacterial translocation because it primarily receives blood from the hepatic portal vein, which is physically connected to the circulations of the gut and the mesenteric and visceral adipose tissues. In addition, the proximity of inflamed visceral adipose tissue during obesity to the portal venous circulation allows released pro-inflammatory cytokines to directly affect the liver, promoting steatoinflammatory reactions. Because CPEB4 depletion under HFD is accompanied by a reduction in the proinflammatory profile of both microbiome and visceral fat depots, we explored the possibility of whether elimination of CPEB4 might decrease the propensity to develop inflammation in the liver as well. CPEB4^{KO} mice exhibited complete loss of CPEB4 protein in the liver (Figure 6A). In contrast to the observed in white adipose tissue, the amount of CPEB4 in the liver was not increased by HFD feeding for 16 weeks. Instead, CPEB4 protein expression tended to be lower in the liver of HFD-fed wild-type mice relative to ND-fed wild-type mice (Figure 6A). Also, we found that CPEB4^{KO} mice receiving dietary fat presented evidence of a less severe inflammatory phenotype and reduced translocation of pro-inflammatory bacteria, as evidenced by the reduction in the expression of markers of bacterial translocation and inflammation, including lipopolysaccharide-binding protein (LBP) and TLR4, in the liver of HFD-fed CPEB4^{KO} mice, compared with wild-type mice on HFD (Figure 6B). Notably, substantial upregulation of CD163, a monocyte/macrophage-specific marker expressed predominantly on cells that possess strong anti-inflammatory potential, was also seen in HFD-fed CPEB4^{KO} mice compared to wild-type controls on the same diet (Figure 6B). In addition, the increased level of alanine transaminase, a common measure for liver injury, observed in the liver of HFD-fed wild-type mice was reduced by ~30% in the absence of CPEB4, although the difference did not reach statistical significance (Figure 6C). These results suggest that the livers of CPEB4^{KO} mice were partially protected against HFD-induced liver inflammation, an effect that could be secondary to the reduction of inflammation in extrahepatic adipose tissues. There was, however, no protection against liver steatosis. Thus, the expected accumulation of excess lipids in hepatocytes after prolonged (4 months) HFD consumption was only minimally and insignificantly reduced after CPEB4 depletion (Figure 6D), and histological comparison (H&E and Oil-Red staining) failed to reveal any difference in the degree of hepatosteatosis (Figure 6E), compared with HFD-fed wild-type mice. There were also no apparent signs of liver fibrosis after HFD feeding for 16 weeks in wild-type and CPEB4^{KO} mice, compared with ND-feed animals, as determined by Sirius Red staining for collagen (Figure 6E,F) and immunoblotting for alpha-smooth muscle actin (a marker of hepatic stellate cell activation and fibrosis) (Figure 6B), and CPEB4 depletion did not induce major changes on these parameters either. Furthermore, the livers from ND-fed CPEB4^{KO} mice were indistinguishable from those of ND-fed wild-type mice (Figure 6E).

4. DISCUSSION

This study demonstrates that the RNA-binding protein CPEB4 represents a new culprit required for the abnormal obesity-associated phenotype and an attractive therapeutic target for treating obesity

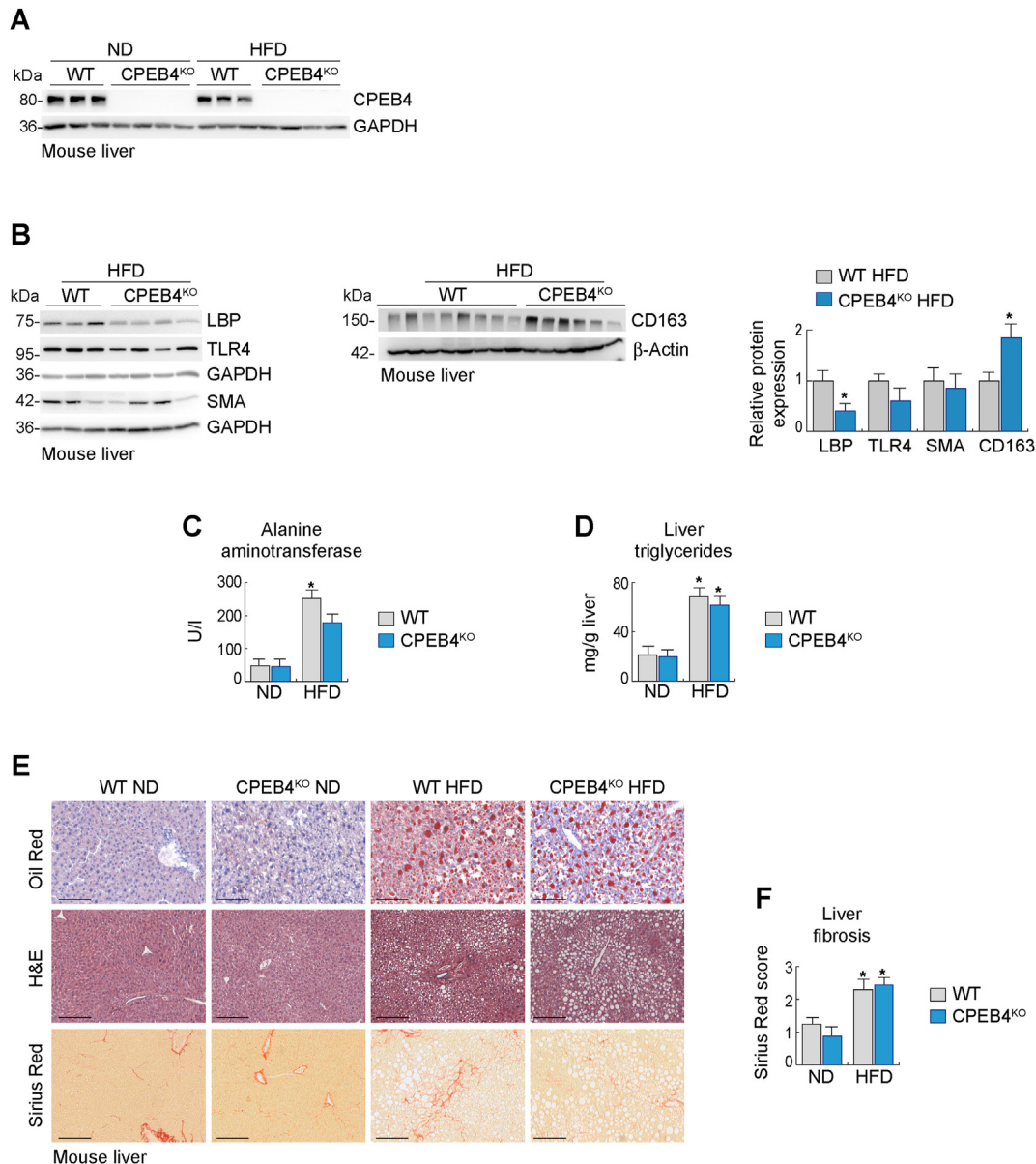


Figure 6: CPEB4 depletion decreases the susceptibility to obesity-related liver inflammation. (A) Hepatic CPEB4 immunoblotting demonstrating effective depletion in CPEB4^{KO} mice. (B) Hepatic expression of LBP, TLR4, SMA and CD163 proteins and quantification. GAPDH or β-actin were used as the loading control. Unprocessed original images of blots are shown in [Supplemental Fig. 7](#). (C) Serum alanine aminotransferase levels measured in CPEB4^{KO} and wild-type mice fed ND (n = 6–7/genotype) or HFD (n = 12–20/genotype). (D) Liver triglyceride levels in CPEB4^{KO} and wild-type mice fed ND (n = 6–7/genotype) or HFD (n = 12–20/genotype). (E) Oil Red, Hematoxylin & Eosin and Sirius Red histological staining in liver sections from CPEB4^{KO} and wild-type mice fed with ND or HFD. (F) Sirius Red quantification in CPEB4^{KO} and wild-type mice fed ND (n = 6–7/genotype) or HFD (n = 12–20/genotype). All values represent the mean ± SEM of independent biological replicates. *P < 0.05 (two-tailed Student's t-test). See also [Supplemental Fig. 7](#).

([Figure 7](#)). The translational implications of these findings in humans are considerable because obesity has reached epidemic proportions worldwide and is a major risk factor for many pathologies.

In the current study, we show that prolonged high-fat feeding augments the expression of CPEB4 in intra-abdominal white adipose depots of both humans and rodents. This overexpressed CPEB4 activates a post-transcriptional regulatory program in obese white adipocytes, through binding to specific CPE elements within noncoding 3'UTRs of selected mRNAs. This program, in turn, triggers translation activation and subsequent protein overexpression of factors that are essential for adipose tissue expansion (such as *Cebpb*, *Stat5a*, and *Klf2*) and the adipocyte-intrinsic immune-like potential (such as *Ccl2*

and *Tlr4*), as demonstrated by next-generation sequencing technologies. Consistently, blocking CPEB4 production interferes with adipocyte differentiation in vitro and decreases visceral adiposity, fat mass gain, and body weight in vivo in CPEB4^{KO} mice fed with an obesogenic diet. In addition, CPEB4 depletion reduces adipose tissue inflammation in HFD-fed mice and decreases the proinflammatory profile of obese adipocytes and their ability to recruit proinflammatory macrophages into obese fat depots. These effects are most likely mediated by the action of CPEB4 within adipocytes based on our in vitro experiments in primary adipocytes and cell lines and in vivo studies showing that mice bearing a targeted deletion of CPEB4 in macrophages do not have a phenotype under obesity conditions. Moreover, for *CCL2* and *TLR4*,

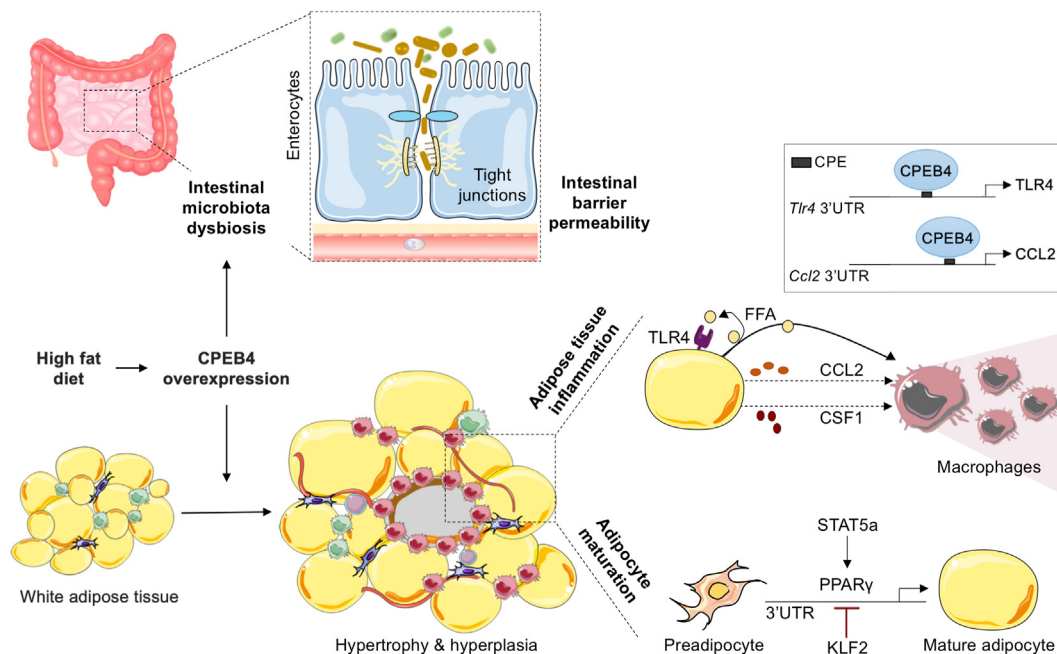


Figure 7: CPEB4-dependent posttranscriptional reprogramming in obese white adipocytes. In this work, we show that cytoplasmic polyadenylation element binding protein 4 (CPEB4), which controls the translation of specific mRNAs by modulating their poly(A) tails, is highly expressed in visceral fat of obese but not lean humans and rodents (mice and rats), where it orchestrates a posttranscriptional reprogramming essential for aggravation of high-fat-diet-induced obesity. Mechanistically, CPEB4 overexpression in obese adipocytes activates the translation of factors essential for adipose tissue expansion (*Cebpb*, *Stat5a*) and for adipocyte-intrinsic immune-like potential (*Ccl2*, *Tlr4*), as demonstrated by RNA-immunoprecipitation and high-throughput sequencing and experimentally validated *in vivo*. Consistently, blocking CPEB4 production in knockout mice protects against diet-induced body weight gain and reduces adipose tissue enlargement and inflammation. In addition, the depletion of CPEB4 specifically in obese adipocytes using short hairpin RNAs decreases cell differentiation, lipid accumulation and the proinflammatory and migratory capacity of macrophages. CPEB4 overexpression during high-fat diet-induced obesity also modulates microbiota towards a more pathogenic profile and regulates tight junction expression, with consequences on intestinal epithelial barrier integrity. These findings identify CPEB4 as a driver and therapeutic target to combat obesity.

which play a unique and central role in attracting macrophages into obese adipose tissue, we do experimentally validate that indeed CPEB4 depletion in HFD-fed *CPEB4*^{KO} mice results in reduced protein levels. These reduced levels of CCL2 and TLR4, in turn, explain the marked attenuation of the obesity-associated adipose tissue inflammatory phenotype observed in the absence of CPEB4. CPEB4 also contributes to the acquisition of a more pathogenetic microbial signature under obesity conditions, which may be related to our recent findings in large-scale microbiome GWAS in humans demonstrating that the locus harboring the *CPEB4* gene on chromosome 5 is associated with variations in microbiota composition. Furthermore, given the upregulation of the expression of tight junction proteins observed in our study upon CPEB4 depletion, it can be assumed that CPEB4 directly regulates the translation and expression of these proteins, thus impairing the intestinal barrier in obesity. These effects could also be secondary to the improvement of obesity-induced dysbiosis caused by CPEB4 ablation and the enrichment in bacteria producing butyrate and other short-chain fatty acids, which enhance intestinal barrier by facilitating tight junction assembly [32,33]. It remains unclear whether a CPEB4-dependent regulation of the localization of tight junction proteins can produce at least some of these changes, as previously observed for CPEB1 [36].

At first sight, our current findings showing that the hepatic steatosis developed after four months of HFD in mice was largely unaffected by CPEB4 depletion may seem to be in disagreement with our recent study showing that CPEB4 depletion exacerbated fatty liver disease after HFD [10]. However, this different hepatic phenotype may be explained by the fact that the impact of CPEB4 on NAFLD is determined

by the duration of the high-fat feeding and by the striking fluctuations of CPEB4 protein expression within the liver along with NAFLD progression. Thus, in response to short-term endoplasmic reticulum stress, CPEB4 is transiently upregulated in hepatocytes through an *elf2 α* -dependent mechanism. This CPEB4 drives a protective response, relying on the activation of the adaptive unfolded protein response to restore cell homeostasis. Accordingly, CPEB4 depletion in this setting is detrimental [10]. In the current study, during prolonged nutrient excess, CPEB4 protein expression within the liver shows no increase and CPEB4 depletion has no detectable effect on steatosis though it attenuates liver inflammation, in addition to all the extrahepatic phenotypic improvements. Therefore, CPEB4 depletion in this pathological setting has beneficial consequences. Recently, CPEB4 depletion has been found to be beneficial in other chronic liver disease scenarios by reducing fibrogenesis [12], and pathological angiogenesis [11].

This study promotes a paradigm shift toward translational control, enormously expanding this area of research and creating newer opportunities to develop better treatments to combat obesity. Our findings strongly suggest that strategies targeting CPEB4 could be useful for counteracting obesity and its sequelae, with translational implications in humans in clinical practice. This is further corroborated by the elevation of CPEB4 expression in visceral fat in obese humans. In addition, CPEB4 signaling is an evolutionally highly conserved mechanism, further validating the translatability of our findings. Furthermore, the unveiled CPEB4-mediated mechanism is essential under obesity conditions, but dispensable for adipose tissue homeostasis, as we have demonstrated through several observations, including low

CPEB4 expression in healthy fat depots but robust CPEB4 over-expression during obesity, and lack of significant effects of CPEB4 depletion on normal diet-fed mice. We highlight that we are currently developing different therapeutic approaches to selectively block the activities of CPEBs, aiming to prevent their binding to target mRNAs in the specific cell types of interest [37]. Hopefully, these CPEB4 inhibitors will make it to the clinic in a near future for preventing and halting obesity and other human diseases.

AUTHOR CONTRIBUTIONS

NP: acquisition and analysis of data. EGP, JG, SNS, AB, CS, MFA, VC, JC, MRP: acquisition of data. OR: RIP-Seq analysis. LT, CB, MR, AF: microbiome analysis. RS, KPR, JT: human tissue samples collection. RM: scientific input and funding. MF: study concept, design, and supervision; analysis of data; writing of manuscript and design of figures; funding acquisition.

CONFLICT OF INTEREST

Authors declare that they have no competing interests.

ACKNOWLEDGMENTS

This work was supported by grants from the FEDER/Spanish Ministry of Science, Innovation and Universities (SAF2014-55473-R, SAF2017-87988-R, PID2020-118937RB-I00 MCIN/AEI/10.13039/501100011033, BES2015-071399 and PRE2018-083718 to MF; BFU2017-83561-P and PID2020-119533 GB-I00 to RM), and the Spanish Association Against Cancer (GCB15152955MEND), Worldwide Cancer Research Foundation (20_0284), World Cancer Research Fund International (IIG_FULL_2020_021), BBVA Foundation (28/2019), La Caixa Foundation (HR18-00302), and La Marató TV3 Foundation (2019–0259) to MF and RM. IDIBAPS and IRB are supported by the CERCA Programme (Catalan Government). IRB is the recipient of a Severo Ochoa Award of Excellence from the Spanish Government. We also thank N. Prats from the Histopathology Facility at IRB, I. Crespo from the IDIBAPS Flow Cytometry and Cell Sorting Facility and A. Bosch from the UB Microscopy Facility for their assistance with analysis.

APPENDIX ASUPPLEMENTARY DATA

Supplementary data to this article can be found online at <https://doi.org/10.1016/j.molmet.2021.101388>.

REFERENCES

- [1] Kopelman, P.G., 2000. Obesity as a medical problem. *Nature* 404(6778):635–643.
- [2] Despres, J.P., Lemieux, I., 2006. Abdominal obesity and metabolic syndrome. *Nature* 444(7121):881–887.
- [3] Weill, L., Belloc, E., Bava, F.A., Mendez, R., 2012. Translational control by changes in poly(A) tail length: recycling mRNAs. *Nature Structural & Molecular Biology* 19(6):577–585.
- [4] Novoa, I., Gallego, J., Ferreira, P.G., Mendez, R., 2010. Mitotic cell cycle progression is regulated by CPEB-dependent translational control. *Nature Cell Biology* 12(5):447–456.
- [5] Belloc, E., Mendez, R., 2008. A deadenylation negative feedback mechanism governs meiotic metaphase arrest. *Nature* 452(7190):1017–1021.
- [6] Pique, M., Lopez, J.M., Foissac, S., Guigo, R., Mendez, R., 2008. A combinatorial code for CPE-mediated translational control. *Cell* 132(3):434–448.
- [7] Ortiz-Zapater, E., Pineda, D., Martinez-Bosch, N., Fernandez-Miranda, G., Iglesias, M., Alameda, F., et al., 2011. Key contribution of CPEB4-mediated translational control to cancer progression. *Nature Medicine* 18(1):83–90.
- [8] Bava, F.A., Eliscovich, C., Ferreira, P.G., Miñana, B., Ben-Dov, C., Guigo, R., et al., 2013. CPEB1 coordinates alternative 3'UTR formation with translational regulation. *Nature* 495(7439):121–125.
- [9] Perez-Guijarro, E., Karras, P., Cifdaloz, M., Martinez-Herranz, R., Cañon, E., Graña, O., et al., 2016. Lineage-specific roles of the cytoplasmic polyadenylation factor CPEB4 in the regulation of melanoma drivers. *Nature Communications* 7:13418.
- [10] Maillo, C., Martin, J., Sebastian, D., Hernandez-Alvarez, M., Garcia-Rocha, M., Reina, O., et al., 2017. Circadian- and UPR-dependent control of CPEB4 mediates a translational response to counteract hepatic steatosis under ER stress. *Nature Cell Biology* 19(2):94–105.
- [11] Calderone, V., Gallego, J., Fernandez-Miranda, G., Garcia-Pras, E., Maillo, C., Berzigotti, A., et al., 2016. Sequential functions of CPEB1 and CPEB4 regulate pathologic expression of VEGF and angiogenesis in chronic liver disease. *Gastroenterology* 150(4):982–997.
- [12] Mejias, M., Gallego, J., Naranjo-Suarez, S., Ramirez, M., Pell, N., Manzano, A., et al., 2020. CPEB4 increases expression of PFKFB3 to induce glycolysis and activate mouse and human hepatic stellate cells, promoting liver fibrosis. *Gastroenterology* 159(1):273–288.
- [13] Parras, A., Anta, H., Santos-Galindo, M., Swarup, V., Elorza, A., Nieto-Gonzalez, J.L., et al., 2018. Autism-like phenotype and risk gene mRNA deadenylation by CPEB4 mis-splicing. *Nature* 560(7719):441–446.
- [14] Manning, A.K., Hivert, M.F., Scott, R.A., Grimsby, J.L., Bouatia-Naji, N., Chen, H., et al., 2012. A genome-wide approach accounting for body mass index identifies genetic variants influencing fasting glycemic traits and insulin resistance. *Nature Genetics* 44(6):659–669.
- [15] Shungin, D., Winkler, T.W., Croteau-Chonka, D.C., Ferreira, T., Locke, A.E., Mägi, R., et al., 2015. New genetic loci link adipose and insulin biology to body fat distribution. *Nature* 518(7538):187–196.
- [16] Huang, H., Fang, M., Jostins, L., Umičević Mirkov, M., Boucher, G., Anderson, C.A., et al., 2017. Fine-mapping inflammatory bowel disease loci to single-variant resolution. *Nature* 547(7662):173–178.
- [17] Jostins, L., Ripke, S., Weersma, R.K., Duerr, R.H., McGovern, D.P., Hui, K.Y., et al., 2012. Host-microbe interactions have shaped the genetic architecture of inflammatory bowel disease. *Nature* 491(7422):119–124.
- [18] Liu, J.Z., van Sommeren, S., Huang, H., Ng, S.C., Alberts, R., Takahashi, A., et al., 2015. Association analyses identify 38 susceptibility loci for inflammatory bowel disease and highlight shared genetic risk across populations. *Nature Genetics* 47(9):979–986.
- [19] Momozawa, Y., Dmitrieva, J., Theatre, E., Deffontaine, V., Rahmouni, S., Charloteaux, B., et al., 2018. IBD risk loci are enriched in multigenic regulatory modules encompassing putative causative genes. *Nature Communications* 9(1):2427.
- [20] Cao, Y., 2013. Angiogenesis and vascular functions in modulation of obesity, adipose metabolism, and insulin sensitivity. *Cell Metabolism* 18(4):478–489.
- [21] Rosen, E.D., MacDougall, O.A., 2006. Adipocyte differentiation from the inside out. *Nature Reviews Molecular Cell Biology* 7(12):885–896.
- [22] Hotamisligil, G.S., 2006. Inflammation and metabolic disorders. *Nature* 444(7121):860–867.
- [23] Kanda, H., Tateya, S., Tamori, Y., Kotani, K., Hiasa, K., Kitazawa, R., et al., 2006. MCP-1 contributes to macrophage infiltration into adipose tissue, insulin resistance, and hepatic steatosis in obesity. *Journal of Clinical Investigation* 116(6):1494–1505.
- [24] Ouyang, W., O'Garra, A., 2019. IL-10 family cytokines IL-10 and IL-22: from basic science to clinical translation. *Immunity* 50(4):871–891.
- [25] Tsukumo, D.M., Carvalho-Filho, M.A., Carvalheira, J.B., Prada, P.O., Hirabara, S.M., Schenka, A.A., et al., 2007. Loss of function mutation in Toll-

- like receptor 4 prevents diet-induced obesity and insulin resistance. *Diabetes* 56(8):1986–1998.
- [26] Thingholm, L.B., Rühlemann, M.C., Koch, M., Fuqua, B., Laucke, G., Boehm, R., et al., 2019. Obese individuals with and without type 2 diabetes show different gut microbial functional capacity and composition. *Cell Host & Microbe* 26(2):252–264.
- [27] Gilbert, J.A., Blaser, M.J., Caporaso, J.G., Jansson, J.K., Lynch, S.V., Knight, R., 2018. Current understanding of the human microbiome. *Nature Medicine* 24(4):392–400.
- [28] Zhao, L., 2013. The gut microbiota and obesity: from correlation to causality. *Nature Reviews Microbiology* 11(9):639–647.
- [29] Rühlemann, M.C., Degenhardt, F., Thingholm, L.B., Wang, J., Skieceviciene, J., Rausch, P., et al., 2018. Application of the distance-based F test in an mGWAS investigating β diversity of intestinal microbiota identifies variants in SLC9A8 (NHE8) and 3 other loci. *Gut Microbes* 9(1):68–75.
- [30] Wang, J., Thingholm, L.B., Skieceviciene, J., Rausch, P., Kummen, M., Hov, J.R., et al., 2016. Genome-wide association analysis identifies variation in vitamin D receptors and other host factors influencing the gut microbiota. *Nature Genetics* 48(11):1396–1406.
- [31] Sanna, S., van Zuydam, N.R., Mahajan, A., Kurilshikov, A., Vich Vila, A., Vösa, U., et al., 2019. Causal relationships among the gut microbiome, short-chain fatty acids, and metabolic diseases. *Nature Genetics* 51(4):600–605.
- [32] Eckburg, P.B., Bik, E.M., Bernstein, C.N., Purdom, E., Dethlefsen, L., Sargent, M., et al., 2005. Diversity of the human intestinal microbial flora. *Science* 308(5728):1635–1638.
- [33] Backhed, F., Ley, R.E., Sonnenburg, J.L., Peterson, D.A., Gordon, J.I., 2005. Host-bacterial mutualism in the human intestine. *Science* 307(5717):1915–1920.
- [34] Clemente, J.C., Ursell, L.K., Parfrey, L.W., Knight, R., 2012. The impact of the gut microbiota on human health: an integrative view. *Cell* 148(6):1258–1270.
- [35] Diehl, G.E., Longman, R.S., Zhang, J.X., Breart, B., Galan, C., Cuesta, A., et al., 2013. Microbiota restricts trafficking of bacteria to mesenteric lymph nodes by CX3CR1hi cells. *Nature* 494(7435):116–120.
- [36] Nagaoka, K., Udagawa, T., Richter, J.D., 2012. CPEB-mediated ZO-1 mRNA localization is required for epithelial tight-junction assembly and cell polarity. *Nature Communications* 3:675.
- [37] Afroz, T., Skrisovska, L., Belloc, E., Guillen-Boixet, J., Mendez, R., Allain, F.H.T., 2014. A flytrap mechanism provides sequence-specific RNA recognition by CPEB proteins. *Genes & Development* 28(13):1498–1514.